

# Synthesis of Silver and Copper Nanowires and Their Application for Transparent Conductors



Conghua Zhou and Yongli Gao

**Abstract** Silver and copper nanowires have been used in many areas, like sensors, catalysis, optoelectronics, etc. They are well-known by the excellent optoelectronic and chemical properties. Here in this chapter, some interesting aspects of these metal nanowires are reviewed, including: (i) the synthesis methods of the metal nanowires; (ii) application of these nanowires in transparent conductors; (iii) application of the transparent conductors in flexible optoelectronic devices, like solar cells, OLEDs, touch screens, transparent heaters, and so on. Besides the applications, this chapter also sheds light to some fundamental problems, including the coarsening dynamics of nanowires, corrosion and protection of nanowires, and also the conducting mechanism of the transparent conductors basing on nanowires. Finally, perspective is given.

**Keywords** AgNWs · CuNWs · Transparent conductor · TC · Transparent and conductive · Solar cells · Flexible

## 1 Introduction

Metal nanowires (NWs) based on gold [1], silver [2], and copper [3], have arisen as a new class of one-dimension (1D) materials that attract ever-increasing attentions due to the excellent optoelectronic and chemical properties. They have been applied widely in transparent conductor (TC, hereafter) [4, 5], conductive composite [6, 7], optoelectronic devices [8], heater [9, 10], catalysis [11–13], and so on. The

---

C. Zhou (✉)

Hunan Key Laboratory of Super-microstructure and Ultrafast Process, Hunan Key Laboratory of Nanophotonics and Device, Institute of Super-Microstructure and Ultrafast Process in Advanced Materials, School of Physics and Electronics, Central South University, Changsha, Hunan 410083, P.R. China  
e-mail: [chzhou@csu.edu.cn](mailto:chzhou@csu.edu.cn)

Y. Gao

Department of Physics and Astronomy, University of Rochester, Rochester, NY 14627, USA

mechanical flexibility of these metal nanowires renders it possible for the application in adaptive optoelectronic devices and wearable electronics [14–16].

The exploration of 1D nanomaterials could be ascribed to the successful synthesis of 0D nanomaterials or nanoparticles [17–20]. Originally in late 1990s, metal based nanowires was synthesized via templating methods, like anodic aluminum oxide (AAO) porous membranes or carbon nanotube (CNT) confined growth [21–23], or DNA chain basing assembly [24]. These methods could help to grow metal based nanostructures from 0 to 1D, though “large-scale” synthesis is somehow difficult to realize. This bottleneck was then broken in the early 2000s, owing to the pioneering works done by Xia et al. (2002). Using the so-called “polyol reaction”, silver nanowires with aspect ratio up to 1000 could be obtained [25–27]. Following the success in synthesis, the silver nanowires were quickly observed to show conductivity of  $0.8 \times 10^5$  S/cm (one eighth of the bulk conductivity of  $6.3 \times 10^5$  S/cm) [25], which triggered the application in TCs that were usually dominated by oxide films like indium tin oxide (ITO) or F-doped tin oxide (FTO). From then on, researches towards the synthesis and application of silver nanowires have bloomed quickly and widely. Such TCs have been used in many optoelectronic devices, like solar cells, touch panels, heaters and so on. Recently, due to the development of wearable electronics, the nanowires are also applied to fabricate flexible and stretchable electrodes under the form of “conductive composite”. Meanwhile, robustness of the nanowire based TCs and composite is discussed due to the long-term use concerns. Questions about the conducting mechanism of such nanowire-based TCs also arise, since the organization mechanism of these TC differs greatly from those oxide-based ones. During the past decade, the synthesis [2, 28, 29], application as TCs (including optoelectronic devices, heaters) [4, 5] or composite [9, 10, 30], and robustness [31] of metal-based NWs have been discussed in several separate reviewing works, though less has been done for the conducting mechanism. In current chapter, the authors will try to put these topics together under the main topic of “nanomaterial and application” designated for the book. In more, the chapter will mainly focus on two kinds of metal nanowires, or silver and copper nanowires (AgNWs and CuNWs). Such consideration is based on the practical availability and the application of them in TCs.

The rest of the chapter is organized as the following: in Sect. 2, the synthesis methods of metal nanowires and the related coarsening dynamics are presented. Section 3 contains the application of these nanowires as TCs, and the application of TCs in optoelectronic devices. Finally, perspective is given in Sect. 4.

## 2 Synthesis of Silver and Copper Nanowires

During the past two decades, several methods have been developed to synthesis metal nanowires, for example polyol method [25–27], solvothermal reaction (including hydrothermal reaction) [32–34], templating [21, 23, 24, 35], and so on, among which

the polyol method and solvothermal reaction are the mostly applied ones. As a result, these two methods are mainly discussed.

## 2.1 Polyol Method of Silver Nanowires (AgNWs)

Polyol method was originally proposed by Fievet and coworkers in 1980s in synthesizing metal particles, like nickel, silver, cobalt, platinum and so on [17, 20]. Micro or submicron sized metal particles could be obtained by reactions using polyol (for example ethylene glycol, diethylene glycol) as solvent and reducing agent, and corresponding salt or metal oxide as metal source. The proposed reaction can be described by formulas (1) and (2) [17, 20]:



whereas M(II) represents related salt or oxide of the metal. Noting that, the reaction could take place even the oxide was less soluble [17].

The reaction process was then developed by Sun et al. (2002) in the synthesis of silver nanowires in the early 2000s. As shown in Fig. 1, with the assistance of the so-called “seeds” of platinum or silver particles, and the coordination effect of polyvinylpyrrolidone (PVP), silver nanowire (AgNWs) with width of about 40 nm and aspect ratio (defined as the ratio between length and width) up to 1000 were successfully obtained. During the reaction, silver nitrite ( $\text{AgNO}_3$ ) and ethylene glycol (EG) were used as the metal source and reducing agent, respectively, following the reaction routines described by formulas (1) and (2) [25]. From the crystallographic study [XRD from Fig. 1d], one can see that these nanowires are of silver. In addition, effects of several parameters were examined with respect to the morphology and aspect ratio of the nanowires, including PVP concentration, reaction temperature, and seeding condition, which will be discussed later. Following that, they also demonstrated the possibility of AgNWs growth without the addition of exotic seeds of platinum particles. With the assistance of PVP and silver nanoparticles seeds (reduced from  $\text{AgNO}_3$  by EG, also marked as the “self-seeding process”), AgNWs with width of ~20 nm (in average) and aspect ratio up to 1000 were harvested. PVP was suggested to act as the coordination reagent in the reaction [26]. It is worth noting that, “seeding” is somehow a rather complicated process. Two year later in 2004, Wiley et al. figured out that hence chloride was present in the reagents of commercial obtained ethylene glycol (EG), depending on the vendor and the lot number. The concentration was from 0.0019 to 0.116 mM [36]. As a result, they suggested that, the previous AgNWs synthesis would have been possibly been contaminated by the hence chloride.

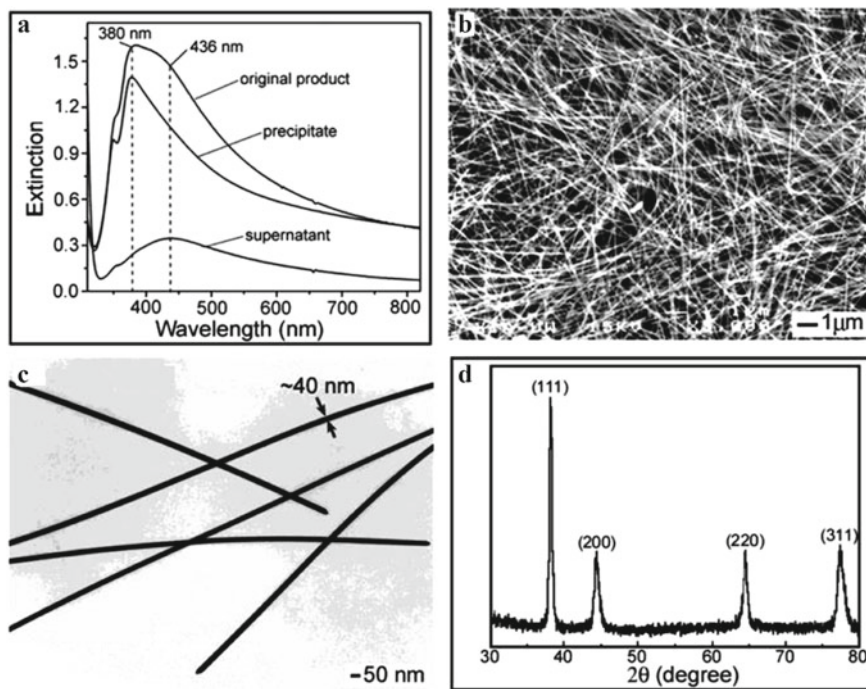


**Fig. 1** **a** UV-visible extinction spectra of the synthesized product; **b** Scanning electron microscopy (SEM) image, **c** transmission electron microscopy (TEM) image, and **d** X-ray diffraction (XRD) pattern of the synthesized silver nanowire (AgNWs). Reproduced with permission [25]. Copyright © 2002, American Chemical Society

Following that, modifications were proposed to the polyol method. For example, in 2012, Lee et al. reported a so-called successive multistep growth (SMG) method in growing very long AgNWs. During the reaction, the obtained AgNWs were purified and used as the “seeds” for the next round of growth, while the reaction followed the similar polyol process described above. After 7 rounds of growth, they could obtain nanowires with length longer than 300  $\mu\text{m}$  (width  $\sim$ 150 nm), and aspect ratio up to 1000–3000. The schematic of this strategy and typical length distribution is shown in Fig. 2 [37]. This study shows that AgNWs could also act as the seeds. Besides that, other methods were also proposed. In 2013, Lee et al. reported a high-pressure polyol method. By controlling the reaction pressure, AgNWs with width of 15–30 nm and length of  $\sim$ 20  $\mu\text{m}$  were obtained. Increasing the reaction pressure could decrease the width of the nanowires. Typically, at pressure of 200 psi ( $1.38 \times 10^6$  Pa), AgNWs with width of 15–22 nm were harvested [32]. As a common synthesis routine of nanomaterials, solvothermal (similar to hydrothermal) reaction was also tried. Jiu et al. (2013) synthesized AgNWs with width of 70 nm and length of 5–20  $\mu\text{m}$  using the solvothermal method, in which  $\text{AgNO}_3$ , PVP and EG were used as the metal source, coordination reagent and reducer, respectively [38]. Then

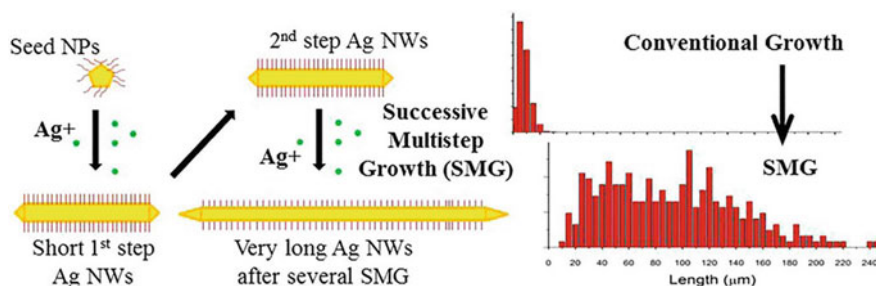


**Fig. 2** Schematic for the successive multistep growth (SMG) and the length distribution of silver nanowires (AgNWs) synthesized from using conventional growth and SMG method. Reproduced with permission [37]. Copyright © 2012, American Chemical Society

in 2016, Xu et al. (2016) showed that, by importing small amount of  $\text{HNO}_3$  in the solvothermal reaction, AgNWs with length longer than 400  $\mu\text{m}$  and average aspect ratio of 821 could be obtained in a one-spot reaction [33]. In such “one-step” growth method the reaction process is greatly simplified, thus the method provides a direct strategy to grow ultra-long AgNWs.

Along with the development of synthesis methods, the crystallographic properties were also studied. With combination of high-resolution transmission electron microscopy (HRTEM) and the selected area electron diffraction (SAED) technique, Xia et al. in 2002 illustrated that, these nanowires were not “single crystalline”, rather, a twinned structure was adopted [25, 27]. One year later in 2003, with the assistance of scanning electron microscopy (SEM) and selected area electron diffraction (SAED), Gao et al. proposed a fivefold twinned structure in the silver nanowire, which was suggested to be bounded by five {100} side planes and capped by five {111} end planes, with growth direction following [110], as is shown in Fig. 3a [39]. Similar results were depicted by Sun, Xia and coworkers in the same year [41]. Following that, in 2005, Gao et al. embedded AgNWs in epoxy and microtomed the matrix into slices with thickness less than 50 nm, by which the cross-section of these nanowires could be directly examined by HRTEM and SEAD. As is shown in Fig. 3b, pentagonal cross-section is clearly depicted. In more, they demonstrated that, the cross-section could hardly be separated into five uniform crystals. Since if that was true, there would be a small region left with angle of  $7.5^\circ$ . However, no such region was observed. Instead, many defects were observed in the boundaries between neighboring twin domains. Accordingly, “fivefold twinned structure” is named, though in fact many defects exist in the twinning boundaries or the “twin planes”. This could also be clearly seen in Fig. 4b [40]. This feature is very interesting, showing that the growth of AgNWs is in fact accompanied by formation of defects. In addition, the growing direction is confirmed to be [110] of the FCC structure. It might be worthy to note that, AgNWs with single crystalline structure were reported to be synthesized by templating method in 2001 [35]. Though the width was as less as few silver atoms (or 0.4 nm). On the other hand, similar five-fold

twinned structure was also believed to be present in CuNWs [11], and even Pd–Au–Pd segmental nanorod [42], pending detailed examination on the cross-section of these nanostructures. However, in 2016 in the atomic study of the Au nanorod, Yu et al. revealed a “necking and breaking” morphological property in the synthesized Au nanorod, and meanwhile many stacking fault defects were disclosed [43]. As a result, it would still be meaningful to verify the relationship between 1D structure formation and defect.

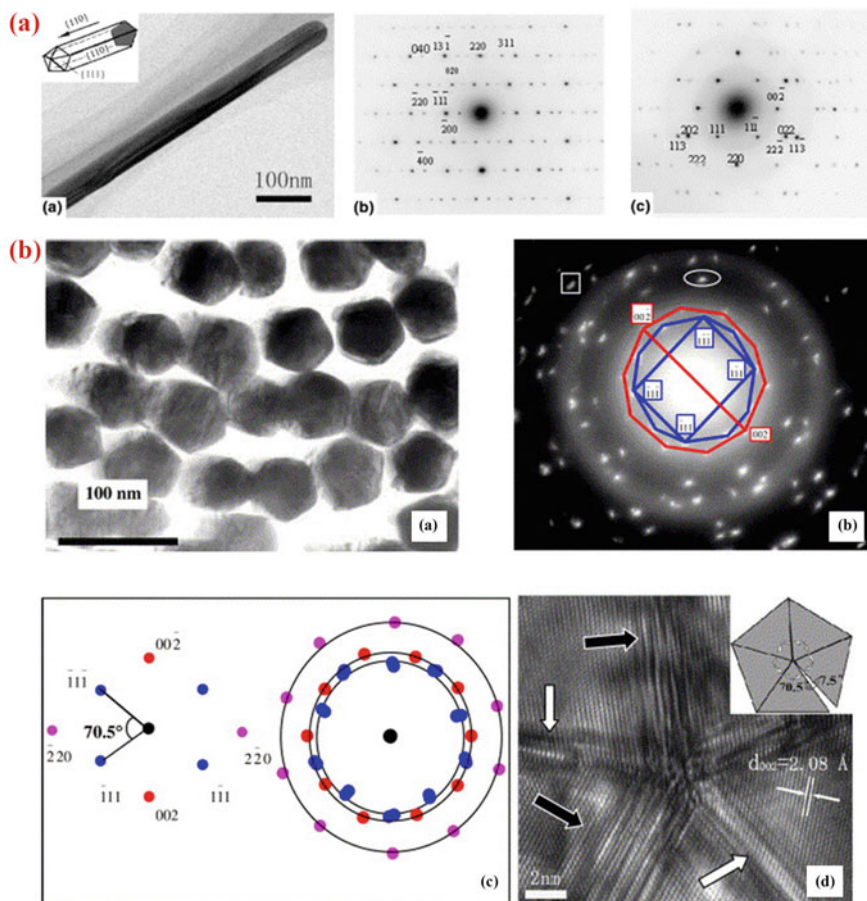


**Fig. 3** **a** Fivefold twinned structure proposed in literature and corresponding selected area electron diffraction (SAED) patterns. Reproduced with permission [39]. Copyright © 2003, Elsevier. **b** Transmission electron microscopy (TEM) image of cross-section of AgNWs, corresponding SAED pattern, and high resolution TEM (HRTEM) image of the cross-section. Clearly, fivefold twinned structure is shown. Reproduced with permission [40]. Copyright © 2004, Elsevier



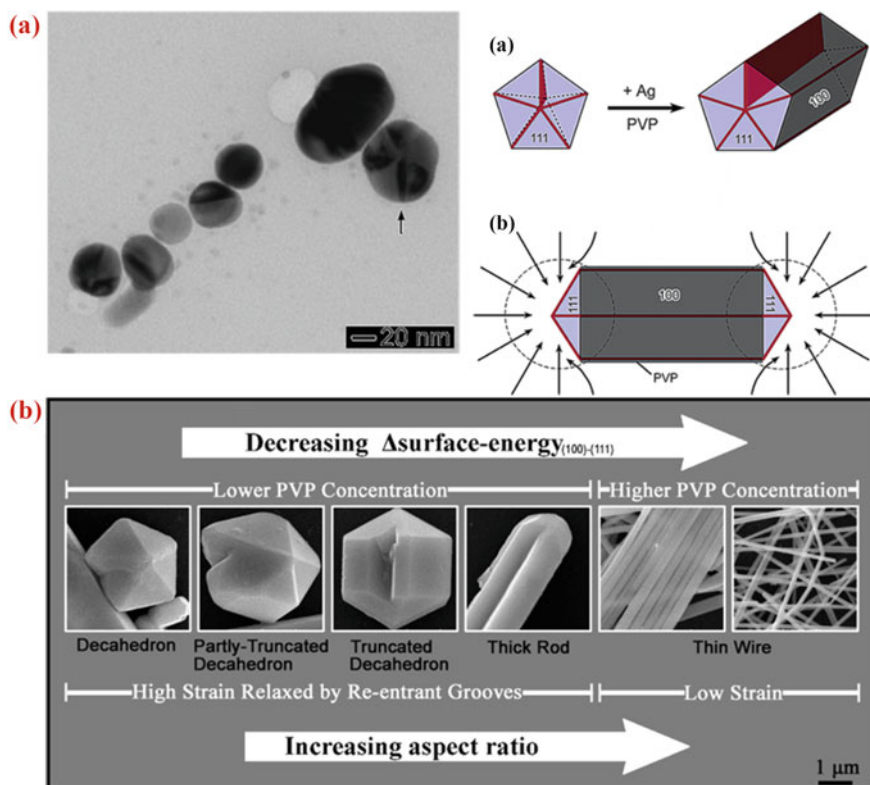


**Fig. 4** **a** TEM image of fivefold twinned silver nanoparticles picked from the solution in polyol growth of AgNWs; and **b** Schematic illustration of the unidirectional growth of twinned silver nanoparticles into AgNWs. The nanowire owns five {100} facets on the side, and ten {111} facets at the end. Heavy capping of PVP molecule on {100} facets is marked by dark grey, while the relative weak capping at the end {111} facets is marked by light-blue color. Reproduced with permission [41]. Copyright © 2003, American Chemical Society. **c** Schematic presentation of the effect of synergy between strain and surface energy difference [ $\Delta\varphi_{\{100\}-\{111\}}$ ] on morphology of the fivefold twinned silver structures. Clearly, when PVP concentration is low, lateral growth is favored; while at higher concentrations, unidirectional growth dominates. Reproduced with permission [51]. Copyright © 2008, American Chemical Society

## 2.2 Coarsening Dynamics of Metal Nanowire

Comparison between the synthesis of 1D metal nanowire and 0D metal particles shows that nanowire growth is different from 0D particles, even though similar reducer and metal source are used [17, 20, 25–27]. Nanowire growth is a unique and dynamic process that can be separated into two distinctive procedures: nucleation and growth. From the ever published literatures, one could find several parameters relating to these two processes, for example, seeds, coordination reagent, reaction temperature and pressure, and even processing techniques. Readers are encouraged to

refer to several reviewing works [2, 28, 29, 44, 45]. Here the main issues are discussed: (i) Transformation of 1D nanowire from 0D seeds; (ii) oxidation behavior during the nanowire growth; (iii) role of precipitation anions.

### 2.2.1 Transformation of 1D Nanowire from 0D Seeds

Seed plays key role in the 1D nanowire growth. Originally, Xia et al. used platinum or silver nanoparticles as the exotic seeds [25], and then “self-seeding” was proposed, in which the seeds were provided by the originally formed silver nanoparticles [26, 27]. As discussed above, fivefold twinned structure is formed in silver nanowire. But works reported in 1990s usually showed the growth of single-crystalline silver nanoparticles [19]. According to previous studies, such single nanoparticles could hardly develop along typical direction that leads to 1D structure. As a result, before nanowire growth, it is crucial to grow seeds (“or nanoparticle”) with similar fivefold-twinned structure like that discussed above. In fact, twinned noble metal particles were observed before the growth of metal nanowires [46–50].

In 2003, following the observation of AgNWs, the seeding process was studied by Sun, Xia et al. In the so-called polyol process, where PVP was used as the coordination molecule, they picked the solution in the starting stage of the reaction, and observed some “fivefold twinned” silver nanoparticles, or the seeds in the system (though not all the particle are twinned). As shown in Fig. 4a, “twin boundaries” are marked [41]. Then they proposed a possible mechanism for 1D AgNWs coarsening. They pointed out three possible stages. At first, the seeds were covered by ten {111} facets, thus decahedral shape was observed. Secondly, defects gathered at boundaries of seeds, make boundaries more attractive place for silver atoms to deposit (after being reduced by polyol reaction), and thus lead to the formation of “nanorods”. Following that, the other five {100} facets appeared. At last, PVP molecules could interact with silver atoms at nanowire surfaces, but the interaction would be stronger at the side {111} facets than that at end facets. The difference between the interaction strength then leads to unidirectional growth of AgNWs. Such processes are clearly depicted in Fig. 5b, whereas the interaction strength is marked by different color. The difference in the interaction strength was confirmed by Zhang et al. [51] Using first-principle calculations basing on density function theory (DFT), the surface energy (eV/atom) was calculated for facets of both {100} and {111}. It was observed that, the surface energy was 0.40724 eV/atom [ $\varphi_{(100)}$ ] and 0.32411 eV/atom [ $\varphi_{(111)}$ ] for pure facets {100} and {111}, respectively; After absorption of  $\alpha$ -pyrrolidone molecule (similar to the unit in PVP), it decreased to be 0.39056 and 0.31755 eV/atom, respectively. As such, the difference between the two, or marked by  $\Delta\varphi_{(100)-(111)}$ , was reduced from 0.08313 to 0.07301 eV/atom. Thus the difference was minimized by 12.2% [51]. However, from the calculated surface energy (though the practical physical chemistry is more complicated) of the two facets, one may expect lateral growth that leads to thick nanowires. Then why usually long and thin AgNWs could be obtained? The authors suggested another possible mechanism, or the confinement of strain. Indeed, from previous studies, it had been known that the nanowires were fivefold twinned.



But the nanowires could hardly be divided into 5 crystals (If not, there should be a small angle of  $7.5^\circ$ ). To fill the gap (according to the small angle region), there in fact existed many defects at the grain boundaries as illustrated by Gao et al. [40]. Similarly, strain was suggested to exist in the nanowires, the thicker was the nanowires, the higher was the strain. In contrast, increment in nanowire length would not add to the strain (given straight nanowire). As a result, a so-called synergy effect was proposed, which is shown in Fig. 5c. When PVP concentration was low, lateral growth dominated due to the relatively high surface energy of facets {100}. Meanwhile the strain of the 1D structure also rose. To release the strain, “re-entrant grooves” appeared. When PVP concentration became higher, passivation happens at the outside facets of {100}, the surface energy difference  $[\Delta\varphi_{(100)-(111)}]$  was then decreased. Then the superiority of lateral growth was reduced, and longitudinal growth happened, since it would not increase the strain of the system. Indeed, the synergy effect provided clear explanation towards the role played by the coordination reagent.

### 2.2.2 Etching Behavior

Up to now, the mostly used metal source in AgNWs growth is  $\text{AgNO}_3$ . Based on the reaction formula (2), a typical formula (3) is expected, in which a byproduct of  $\text{HNO}_3$  appears. Due to the pristine oxidization behavior formula (4) could be anticipated, though later could be seen, the oxidization behavior might be sensitive to the concentration of nitric acid. Such phenomenon was disclosed two years later after the successful growth of AgNWs, along with the two possible reaction formulas listed as following [36, 52]:

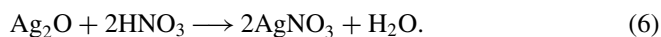


Accordingly, oxidization becomes an important issue in nanowire growth. Wiley et al. (2014) observed that oxygen played a key role in the coarsening dynamics of silver nanostructures. They added trace amount of  $\text{NaCl}$  (0.22 mM) in the typical polyol reaction, and observed two kinds of silver nanoparticles: single crystal and multi-twinned particles in the starting stage of the reaction. Different products were observed when oxygen was expelled or not from the reaction or not [36]. Concretely, in presence of oxygen, only silver cubes and tetrahedrons were obtained. After oxygen was excluded and replaced by argon (Ar) gas, thin and long AgNWs were harvested. Accordingly, they proposed a etching couple made of “ $\text{O}_2/\text{Cl}^-$ ” and suggested that, the originally formed multi-twinned silver particles could be easily be etched by this couple, thus nanowires could be less productive; After oxygen is expelled, the etching effect disappeared, and the seeds could grow into nanowires. At the same time, they fingered out the chloride contamination problem in previous AgNWs synthesis work (as stated in previous section). Indeed, this work drew the

attention to the effect of  $O_2$ , chloride to AgNWs formation at the first time, though the exact etching mechanism would be more complicated. One year later in 2005, Xia et al. added HCl in the polyol reaction (with HCl concentration of 0.125, 0.25 and 0.375 mM, respectively), and studied the effect of HCl concentration on the resultant silver nanostructures [52]. It was observed that, at concentration of 0.125 mM, both silver particles and nanowires were obtained. While silver nanocubes were obtained at concentration of 0.25 mM, and thick wires and irregular particles came out as the concentration increased to 0.375 mM. Similarly, they attributed the formation of cube (at case of 0.25 mM) to the etching effect brought by " $O_2/Cl^-$ ". From the above two studies one could know the important role of "etching" in the growing dynamics of silver nanostructures.

To verify the exact mechanism, more works were done after that. In 2008, Zhang, Tang and coworkers focused on the acidic etching behavior of the byproduct of  $HNO_3$  [according to formula (3)]. To retard the etching behavior, they added steel plates into the polyol reaction, and obtained AgNWs in high concentration (0.5 M) [53]. In 2016, Xu and Zhou et al. studied the effect of  $HNO_3$  in AgNW growth in solvothermal reaction. By adding small amount of  $HNO_3$  in the reaction, they observed 50-fold increase in nanowire length, reaching  $>400 \mu m$  [33]. In order to study the role of  $HNO_3$ , they designed 16 batches of experiments, 8 for reaction with addition of  $HNO_3$  but with varied reaction period, while the other 8 for references (W/O  $HNO_3$ ). This designation eliminated the disruption that might be drawn by "picking" itself. Then, the samples were examined by both UV-Visible extinction spectra and SEM techniques, with photo-images taken at the same time.

As shown in Fig. 5a, b, when there was no  $HNO_3$  added, three cyclic round color changes appeared in the solution. For example, it changed from dark red (1 h) to colorless (4 h) at the first cycle, then turned back to grey at 5 h, but clear again at 6 h. When  $HNO_3$  was pre-added, different behavior was observed. The solution remained colorless for the first 5 h, and changed gradually to brown. Extinction behavior and morphological properties (SEM images could be referred to the literature [33]) showed that, in each cycle, AgNWs and nanoparticles appeared at first, and then disappeared. This implied that, dissolution happened. To explain the beneath mechanism, they carefully examined the reaction environment, and proposed that oxygen played a key role in the reaction. Indeed, there exists less  $O_2$  in the upper space of the autoclave, calculated to be 2.7 mM given that  $O_2$  could be all dissolved in the solution. This concentration was about 11% of [Ag]. Considering the byproduct of  $HNO_3$ , then following reactions could possibly take place, as represented by formulas (5) and (6):



As such, nanowires could grow steadily only after the consumption of  $O_2$ , which is quite similar to that stated by Xia et al. (2004), whereas  $O_2$  was expelled and Ar

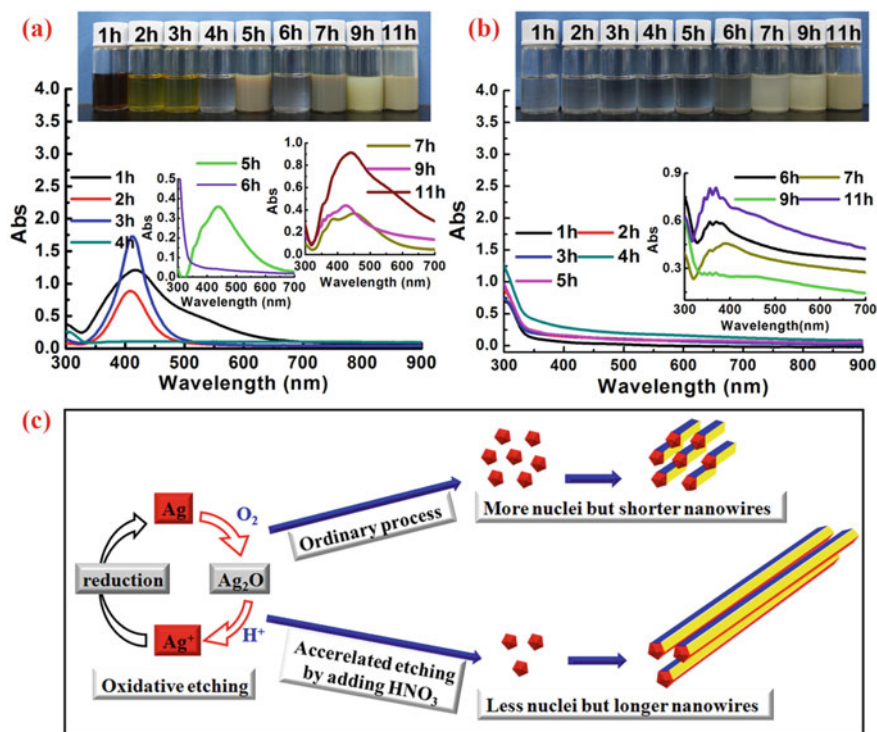


**Fig. 5** UV-Visible spectra of solution obtained from solvothermal reaction at different reacting time: **a** W/O HNO<sub>3</sub>, **b** with HNO<sub>3</sub> (1.44 mM). **c** Schematic of the oxidative etching behavior brought by the etching couple of "O<sub>2</sub>/H<sup>+</sup>", and the effect on long AgNWs growth [33]

was imported as the protection gas [36]. Moreover, it is worthy to note that, to verify the acidic behavior of HNO<sub>3</sub>, specific experiments were designated (refer to literature [33]), showing that when concentration of HNO<sub>3</sub> was low, acidic role appeared, rather than the oxidation behavior. Accordingly, after HNO<sub>3</sub> was added, a screening effect appears. After addition of small amount of HNO<sub>3</sub>, etching behavior brought by the couple of "O<sub>2</sub>/H<sup>+</sup>" could dissolve certain amount of multi-twinned silver nanoparticles or seeds. Then the existing seeds could find more opportunity to grow longer, as depicted schematically in Fig. 5c.

### 2.2.3 Role of Precipitating Anions

Besides PVP, O<sub>2</sub>, HNO<sub>3</sub>, AgNW growth is also affected by anions in the reaction system. AgNWs have been successfully synthesized in solution containing Cl<sup>-</sup> [27], Br<sup>-</sup> [54], S<sup>2-</sup> [55, 56], etc. These anions were found to affect both nanowire width and aspect ratio. Usually, incorporation of Br<sup>-</sup> was favorable for thin nanowire growth. For example, in the so-called high pressure polyol method, Lee et al. (2013) observed

that, mixture of NaCl and KBr was helpful to obtain AgNWs with thickness low to 15–22 nm [32]. Then, Li et al. (2015) showed, by tuning reacting procedure and also the concentration of  $\text{Br}^-$  in polyol reaction, AgNWs with diameters of 20 nm and aspect ratios up to 2000 could be obtained [54]. The effect of  $\text{Br}^-$  concentration on the nanowire width is clearly depicted in Fig. 6. If only  $\text{Cl}^-$  exists, nanowire width is  $72 \pm 15$  nm, after incorporating small portion of NaBr (2.2 mM), the width decreases to  $20 \pm 2$  nm. However, increasing concentration up to 4.4 mM results in particles for the most. As such, anions should play important roles in those reactions. To explore the cause, the authors suggested that, the  $\text{Br}^-$  adsorbed on the AgNWs surface could reduce the coarsening rate perpendicular to nanowire length [32, 57]. However, the detailed mechanism was not clear yet. One possible cause might arise from the “precipitation behavior” brought by the halide anions. It is well-known that, halide anions like  $\text{Cl}^-$  and  $\text{Br}^-$  could react with  $\text{Ag}^+$  and get precipitates; in more, AgBr is less dissolvable than AgCl. As such, when adsorbed on AgNW surface,  $\text{Br}^-$  could provide stronger protection for the nanowires. As such, it not only prevents the further Ag atom deposition on the surface (for transverse growth), but also makes it more robust when facing with corrosive and oxidizative reagents in the solution. However, more works are needed to clarify this assumption.

### 2.3 Synthesis of Copper Nanowires

Copper nanowires (CuNWs) have also been synthesized. Toimil Molares et al. (2013) demonstrated that CuNWs with width of 30–60 nm could be grown by electrochemical method [58]. Shi et al. (2015) synthesized CuNWs from hydrothermal reaction (120–180 °C, 48 h) containing  $\text{CuCl}_2$ , octadecylamine (ODA) [59]. CuNWs with width of 50–100 nm, and aspect ratio up to  $10^5$  were obtained by this one pot reaction. In more, reaction temperature was observed to affect nanowire growth. 120 °C reaction helped to obtain uniform distribution in nanowire width (30–50 nm), while 180 °C reaction produced wider distribution (or 50–1000 nm) and meanwhile reduced aspect ratio. They suggested that ODA played a key role in nanowire growth. It could serve as both of the reducing agent and the coordination reagent. The reduction behavior was easily to distinguish by judge the production from reaction. As for the coordination reagent, ODA molecules were suggested to coordinate with Cu (II) cations. They noticed that, since ODA molecules could be hardly dissolved by water, these molecules tended to form micelles with lamellar structure. Such micelle could serve as “micro-reactor”, in which 1D CuNWs could grow separately. Similar “micelle-derived” growth mechanism was proposed later. For example, Zhang et al. (2015) proposed a growth model basing on “liquid-crystalline medium”. During the reaction, HDA and cetyltrimonium bromide (CTAB) were mixed at first. At elevated temperatures, this mixture will form a liquid-crystalline medium. Then copper source, or copper acetylacetonate  $[\text{Cu}(\text{acac})_2]$  was added and reacted, with presence of Pt catalyst in the medium [60]. The growth dynamics are shown in Fig. 7a. They suggested that, due to the coordination behavior between Cu salt and  $\text{Br}^-$  (from

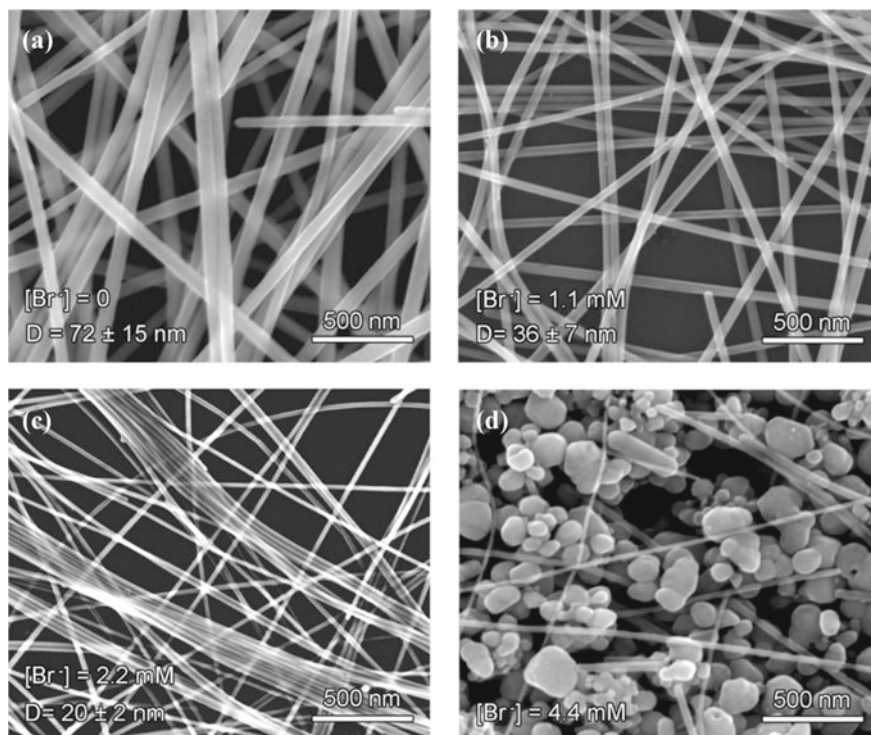


**Fig. 6** Effect of concentration of NaBr on AgNWs width (mM): **a** 0, **b** 1.1, **c** 2.2 and **d** 4.4. Concentration of other reagents was kept the same, or 26.5, 50.5 and 4.2 mM, for AgNO<sub>3</sub>, PVP and NaCl, respectively. Reproduced with permission [54]. Copyright © 2015, American Chemical Society

CTAB) and HDA, the added Cu precursor molecules could fill the tubular channels of the pre-formed liquid-crystallines. After reduced by HDA, the Cu atoms were mounted to nanowires. Due to the preferential adsorption of HAD and Br<sup>-</sup> on {200} planes, unidirectional growth is favored at [110] direction. CTAB and Pt catalyst were found to play important role in nanowire formation. When CTAB concentration was relatively low, only polyhedrals were obtained. On the other hand, without addition of Pt, neither nanowires nor nanoparticles were observed even after 10 h reaction. It is worthy to note that, according to the authors, single crystalline-like CuNWs, with hexagonal cross-section were obtained. This is different from those AgNWs, releasing an open question. Other methods were also imported for CuNW growth. For example and also shown in Fig. 7b, copper nanowires (CuNWs) with width of 17.5 nm and aspect ratio of 1000 were reported by Cui et al. (2015) [61], using tris(trimethylsilyl)silane, oleylamine (OLA) and CuCl<sub>2</sub> as the reducing reagent, coordinating ligand and metal source, respectively. The reaction routine was similar to that used in AgNWs growth, though with different reducing reagent and coordination ligand. The coordination behavior between OLA and Cu(II) was suggested to



play a key role in 1D structure formation [61]. Besides, Jin et al. (2015) synthesized CuNWs in oil bath (100 °C for 6 h), using glucose, hexadecylamine (HDA) as reducer and capping agent [also, to coordinate with Cu(II)], respectively [62]. CuNWs with width of  $24 \pm 4$  nm, and length from tens to hundreds of micrometers were harvested. Moreover, these works also demonstrated the application of nanowires in transparent conductors (TCs), which will be discussed later [60, 61].

From above description, one could find that reacting routine of CuNW is similar to AgNW. Both of them contain metal salts, reducers, and capping (coordinating) agents, though the detailed materials are different from each other. In addition, coordination agent plays a key role in the reactions. It could coordinate with metal atoms, thus reduce the surface energy of side planes and prompt unidirectional growth of nanowires.

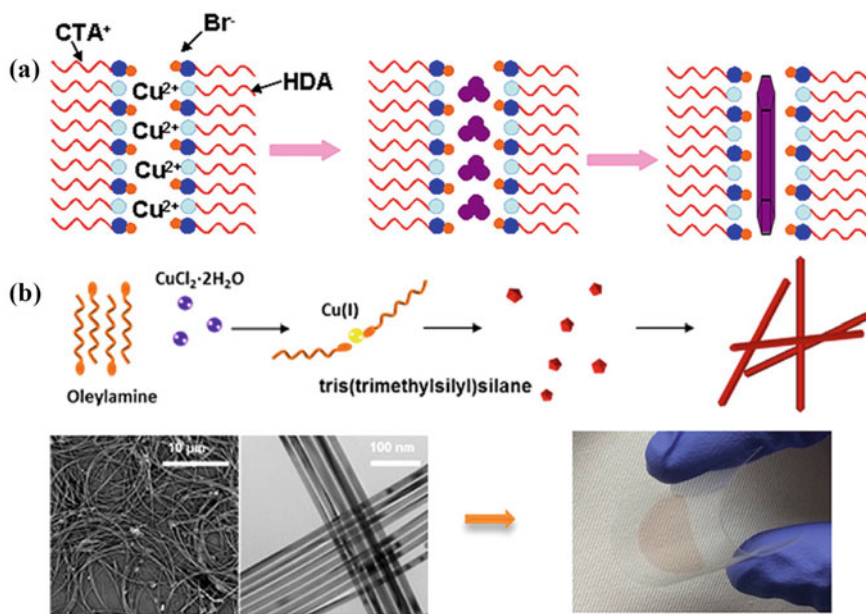


**Fig. 7** **a** Formation scheme of CuNWs in liquid-crystalline medium. Reproduced with permission [60]. Copyright © 2012 American Chemical Society. **b** Schematic for the growth of ultrathin copper nanowires (CuNWs), and corresponding SEM image, TEM images of the synthesized CuNWs, and typical TC prepared from the nanowires. Reproduced with permission [61]. Copyright © 2015, American Chemical Society



## 2.4 Summary

In this section, synthesis routines of AgNWs and CuNWs are described, including the synthesis methods, coarsening mechanisms of nanowires, as well as the nanowire structural properties. Honestly, there still remain some interesting questions to answer: (i) What causes the formation of the five-fold seeds and then the nanowires? (ii) Could single crystalline AgNWs be realized? (iii) What is the exact role played by halide anions in the growth of AgNWs? More works are needed to clarify those mechanisms.

## 3 Application of Metal Nanowires in Transparent Conductors

One of the applications of these metal nanowires is the transparent & conductive film (TCs). Nowadays the commercialized TCs are mainly basing on oxide films, like ITO or FTO. They have shown excellent optoelectronic performance, though with relatively poorer flexibility. Metal nanowires is flexible, thus could solve this problem. Since the first attempt in TCs done by Lee et al. [63], researches on nanowire network basing TCs widespread, as well as the application in optoelectronic devices. In this section, these aspects will be all introduced, in addition, conducting mechanism of the networks, and protection method are also covered. Prior to detailed discussion on these aspects, it would be meaningful to list typical progress during the last decade in TCs made of nanowires, with respect to preparation methods, treatment and corresponding optoelectronic performances. Two tables are summarized as Tables 1 and 2, for AgNWs and CuNWs, respectively. It is worthy to note that, for both of these two kinds of nanowires, T% of 90%, and  $R_{sh}$  of 5–30  $\Omega/\square$  have been achieved on both rigid and flexible substrates, which is comparable to ITO based TCs.

### 3.1 Preparation of TC

As noted above in 2008, Lee et al. reported a kind of AgNW basing TCs, with transmittance ( $T\%$  at 550 nm) of 84%, and sheet resistance ( $R_{sh}$ ) of 10.3  $\Omega/\square$  or ( $\Omega/\square$ ). Typical SEM images, effect of annealing period on sheet resistance of AgNWs films, and typical UV–Visible transmission spectra of AgNWs basing TCs are shown in Fig. 8a–c. When prepared on flexible substrate (Kapton tape), the film conductance only changed 1% after bending the substrate (along with the network deposited on) to radii of 4 mm. Also, effect of contact resistance between nanowires was noticed, and heating was performed to decrease the resistance. Effect of nanowire density on the film conductance was also studied [inset of Fig. 8c] [63]. Moreover, they showed power conversion efficiency (PCE) of 0.38% for organic photovoltaic solar

**Table 1** Optoelectronic performance of AgNWs based TCs

	T (%) <sup>a</sup>	Rsh ( $\Omega/\square$ )	Haze (%)	Coating method	Substrate	Treatment	Year
Ag	84 <sup>b</sup>	10.3	–	Spin coating	Glass	Heating <sup>c</sup>	2008 [63]
Ag	95	580	–	Spray coating	Saran wrap	Plasma	2012 [64]
Ag	90 85	19 47.78	–	Transfer	Glass Plast <sup>c</sup>	Heating	2012 [65]
Ag	88	40	$\leq 1$	Casting	PET	–	2013 [32]
Ag	89.4	14.9	–	Spin coating	Glass	Plasma/AgNPs	2014 [66]
Ag	92	5	7.26	Roll to roll	PET	Solution bath	2014 [67]
Ag	99.1 93 <sup>b</sup>	130.0 25 <sup>b</sup>	–	Meyer rod	Glass	Dry <sup>c</sup>	2015 [54]
Ag	90.2	12.5	–	Spin coating	PET	Bending	2015 [68]
Ag	92.6	35.0	–	Spin coating	PET	NaBH <sub>4</sub>	2018 [69]
Ag	95	28	1.2	Transfer	Glass	NaBH <sub>4</sub>	2018 [70]
Ag	94	30	–	Meyer	PET	Dry <sup>d</sup>	2020 [71]

<sup>a</sup>Measured at wavelength of 550 nm; <sup>b</sup>estimated from the figure of corresponding literatures <sup>c</sup>“heating” is used when temperature is higher than 150 °C in the reported document, otherwise, dry is noted; <sup>d</sup>According to the literature, the fabricated AgNWs TCs are rinsed by ethyl alcohol and DI respective

**Table 2** Optoelectronic performance of CuNWs based TCs

	T (%) <sup>a</sup>	Rsh ( $\Omega/\square$ )	Haze (%)	Coating method	Substra-te	Treatment	Year
Cu	90	90	–	Transfer	Glass	Heating	2012 [60]
Cu	90	34.8	2–3	Transfer	Glass	Heating	2015 [61]
Cu	85.5	19.8	–	Spray	–	Heating	2016 [72]
Cu	83.0	24.5	–	Roll to roll	PC <sup>b</sup>	Pulse light	2016 [73]
Cu	89.3	28.2	~2	Transfer	Glass	Cu@r-GO	2016 [74]
Cu	89	35	<3	Transfer	Glass	Cu@Au	2018 [75]
Cu	70.2 <sup>c</sup>	24	–	Transfer	PC <sup>b</sup>	Heating	2018 [76]
Cu	87	33	–	Transfer	Glass	Pulse laser	2020 [77]

<sup>a</sup>Measured at wavelength of 550 nm; <sup>b</sup>polycarbonate; <sup>c</sup> the T% was measured containing substrate

cells using such network as bottom electrode [inset of Fig. 7d]. Indeed, this work opened a door for the metal nanowires to participate in the fast development progress of optoelectronics. Following that, many state-of-art strategies have been developed, for the fabrication of nanowire basing TCs, the methods to enhance the optoelectronic performance of such TCs, and the application of the TCs in optoelectronic devices. For the sake of organization, the device applications will be discussed separately.

In laboratory, nanowire basing TCs were usually fabricated by spin-coating method, which it is applicable for small area preparation. Roll-to-roll method might be more suitable for mass production. In 2014, Lee et al. reported a “roll-to-roll” routine for AgNW TC [67]. As shown schematically in Fig. 9a, 3 distinct steps were involved in this strategy. At first (step 1), AgNWs were coated on flexible plastic substrate (like PET) by “Meyer rod” method, and transferred to a “solvent spray system”, where several kinds of solvents could be used, like distilled water, methylene chloride and tetrahydrofuran. Then (step 2), the TC (along with substrate) were laminated by two rollers to weld the nanowires. At last, the compressed TCs were rinsed by NaCl and FeCl<sub>2</sub> solution, and finally by distilled water. Such fabrication routine holds four aspects of merits: (i) the method is suitable for scalable production due to fluent treating processes; (ii) Contact resistance between nanowires could be

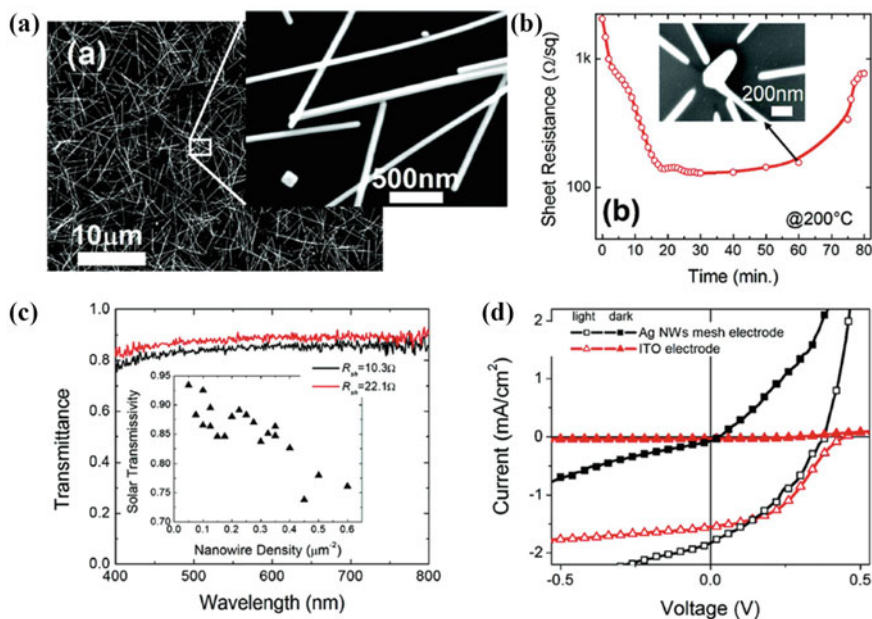


**Fig. 8** **a** SEM images of AgNWs film on silicon substrates. **b** Effect of annealing period on sheet resistance of AgNWs films. **c** Typical UV—Visible transmission spectra of AgNWs TCs with two kinds of  $R_{sh}$  of 22.1 and 10.3  $\Omega/\square$ . Inset shows the effect of nanowire density on T%. **d** Typical current density—voltage (J-V) curves of organic photovoltaic solar cells prepared on ITO and AgNWs TCs. Reproduced with permission [63]. Copyright © 2008, American Chemical Society

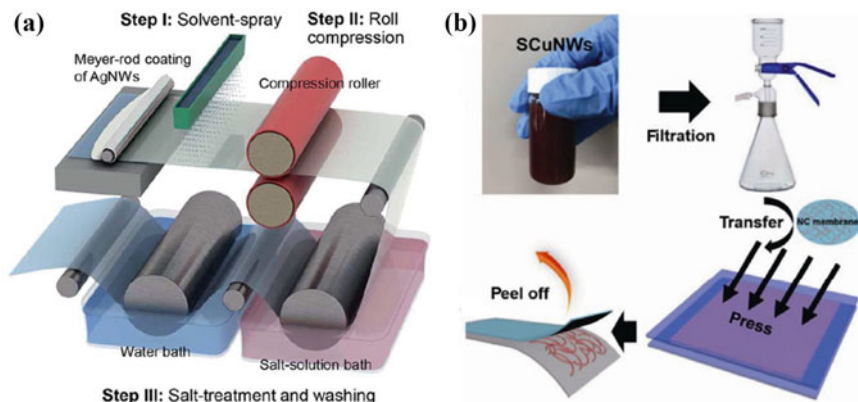


**Fig. 9** **a** Schematic of roll-to-roll (R2R) coating method for the fabrication of AgNWs TCs. Reproduced with permission [67]. Copyright 2009, Royal Society of Chemistry. **b** Schematic of spray coating used in fabricating CuNWs TC. Reproduced with permission [78]. Copyright © 2018, Springer Nature

largely reduced and thus excellent optoelectronic performance could be obtained due to the compression technique and solution bath. For example, 92% of  $T\%$  and  $5 \Omega/\square$  of  $R_{sh}$  were obtained on flexible plastic substrate, even without high temperature annealing. (iii) Also due to the compression technique, TC surface could be flattened which is quite important for the following optoelectronic device preparation. (iv) This method is compatible to the scalable fabrication of the flexible optoelectronic devices like solar cells, or OLEDs. Anyway, the haze could be decreased by using thin nanowires. Besides roll-to-roll, “transfer” method was also proposed. As shown in Fig. 9b, Zhang et al. used a 3-step transfer method to prepare CuNWs TCs [78]. The first step is filtration in which the nanowire containing “solution” (exactly, it should be named as turbid liquid) was filtrated by a porous membrane. After that, network could be formed between the remaining nanowires on the membrane. The second step is “transfer”, or the formed networks are transferred to a substrate. At last, the transferred networks were annealed. After that,  $T\%$  of 96.65%, and  $R_{sh}$  of  $115.45 \Omega/\square$  was obtained on PET substrate, while the haze was as low as 1.5% due to the ultrathin width of 15 nm.

### 3.2 Methods to Upgrade the Optoelectronic Performance

Normally, there exists a compromise between  $T\%$  and  $R_{sh}$  of TCs. Given certain kind of conductive material, high  $T\%$  usually leads to high  $R_{sh}$ . This is obeyed by nanowire based TCs. As a result, the enhancement in the optoelectronic performance always account on the reduction of  $R_{sh}$  at given  $T\%$ . Such topic is directed to the

conducting mechanism of such nanowire based networks. Usually, the film conductivity is relating the aspect ratio of nanowires, nanowire width and also the contact resistance between nanowires. As seen in literatures, and also the following discussions, longer nanowires are useful in providing more conducting paths, thus favoring the film conductivity. Thus one possible strategy is to synthesis high aspect ratio nanowires, which represents an important sub-topic in the field, and could be refer to several interesting literatures [33, 37, 65, 68, 70, 78–80]. Here we would like to pay more attention to the reduction on contact resistance.

Due to the loose stacking of nanowires, the contact between neighboring nanowires is hardly close enough; meanwhile, organic ligands may cap nanowires. As a result, large contact resistance exists. In 2016, Selzer et al. measured the contact resistance through the junction made by cross-linking nanowires, and showed that the resistance ranged from dozens to several hundreds of ohm for a junction, which is far too larger than the nanowire itself (for example, about  $4.4 \Omega/\mu\text{m}$  for AgNW with diameter of 90 nm) [82]. As a result, it is crucial to enhance the contact between nanowires.

In 2012, Garnett et al. showed that, silver nanowires could be welded by light induced plasmas [64]. As shown in Fig. 10a, they used a broadband tungsten-halogen lamp to irradiate the AgNWs network for 10–120 s, and then examined morphological properties near the junctions. Before illumination, loose stack could be seen. After illumination, welding behavior appeared at the junction region. Furthermore, they performed finite element method simulation on the optical heat generation between nanowires. As being demonstrated in Fig. 10a, heat is mainly generated in the bottom nanowires. Such melting behavior is appealing for junction resistance reduction, making the network a unit. Following that, similar welding techniques were developed, for example, laser [83], intense-pulsed light [84, 85], and pulsed UV laser irradiation [77].

Besides plasma welding, joule heat was also proposed. As shown in Fig. 10b, Song et al. (2014) demonstrated that, by applying suitable current across the AgNWs TC for short period (timescale of tens of seconds),  $R_{\text{sh}}$  could be cut down quickly. Careful examination showed that the contact region between nanowires could be welded [81], like that obtained by Garnett et al. (2012) [64]. They ascribed the welding effect to the synergy between thermal treatment and electro-migration. With assistance of simulation and conductivity measurement, they found that the contact resistance was quite larger than that of AgNW itself. In such situation, the joule heat mainly distributed at the contact region. Since noble atoms were originally found to diffuse easily (with surface diffusion activation energy of  $<1 \text{ eV}$  [81, 86]), welding effect could be harvested under heating, between contact region. The study provides an efficient strategy to reduce contact resistance. However, joule heating was also noticed to cause break down in nanowire TCs, which is due to the unevenly distributed contact resistance, and the high surface energy of nanowire (especially for thinner nanowires) [87–89]. As such, protection is needed [90], as will be discussed later.

In order to reduce contact resistance, nanowire surface should be highlighted. In the original works towards AgNWs basing TCs, the surfactant of PVP remaining from the polyol method synthesis was noticed to hinder the network conductivity [63, 64].

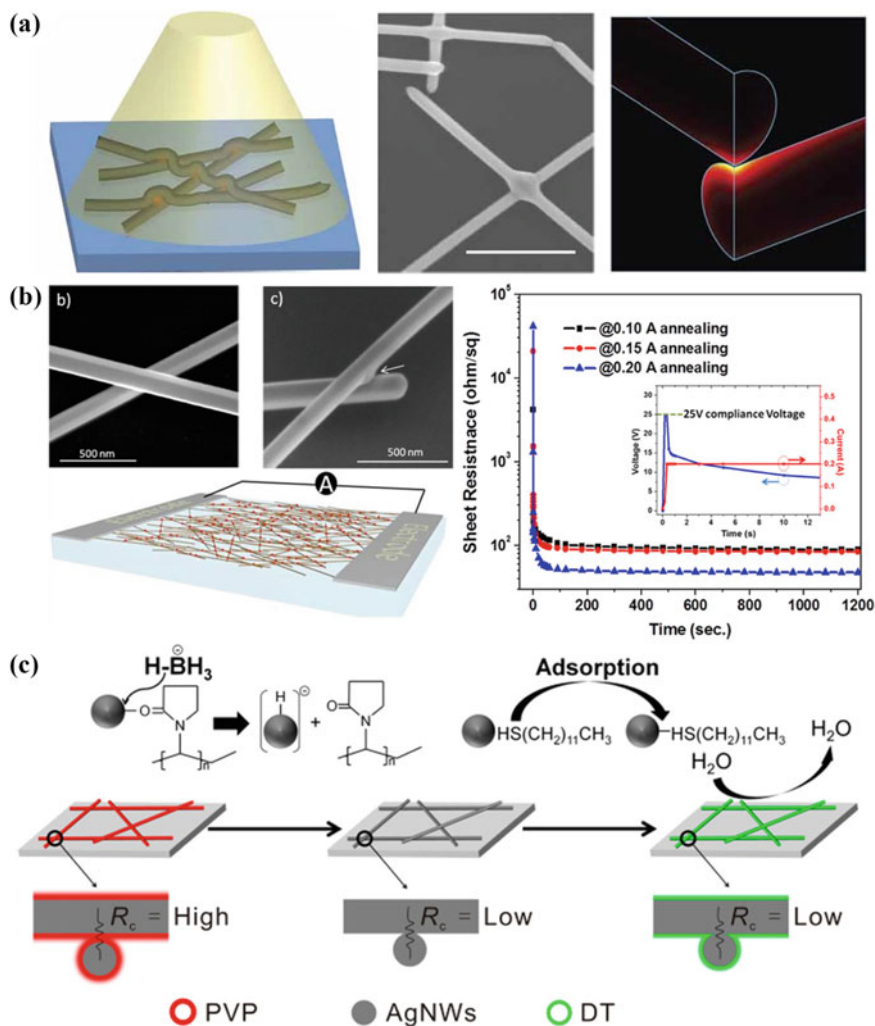


**Fig. 10** **a** Plasma treatment on AgNWs networks: schematic of the treatment, enlarged contact region after the treatment, and finite-element method simulation the treatment are shown. One can see that heat is mainly generated from the bottom nanowire. Reproduced with permission [64]. Copyright © 2019, Springer Nature. **b** Welding AgNWs by current induced joule heating. Equipment for joule heating on AgNWs TC, SEM image of the contacting region, and the effect of treating period on  $R_{sh}$  of TC is shown. Reproduced with permission [81]. Copyright©2014, American Chemical Society. **c** Schematic for the "Room temperature welding" on AgNWs TCs: typically, PVP ligands could be removed from AgNWs by borohydride ( $\text{NaBH}_4$ ). Reproduced with permission [69]. Copyright © 2018, American Chemical Society



Thus such ligands should be moved away. Indeed, this was usually done by multi-time rinsing process. In 2018, Ge et al. proposed an idea of “room temperature welding” between silver nanowires, which was realized through replacing PVP ligands by borohydride ( $\text{NaBH}_4$ ) [69]. As shown in Fig. 10c, the replacement is dominated by the competition of binding energy between silver atom and different ligands. According to the authors, it is about 50.9 kcal/mol for “Ag–O” bond (O is from PVP), while 81.71 kcal/mol between Ag atom and hydride ion (which is caused by the decomposition of  $\text{NaBH}_4$ ). Thus the insulating PVP ligands could be replaced by the hydride ions, which helps to form atom-level-clean interface between neighboring AgNWs, by which “room temperature welding” was obtained. Such welding effect helped to decrease  $R_{sh}$  from 81.5 to 35.0  $\Omega/\square$  (T% at 92.6%). Moreover, another capping layer of hydrophobic dodecanethiol [or DT, in Fig. 9c] was observed to improve the stability of the TCs. This work clearly indicates that: (i) PVP could be hardly completely washed off by common solvent due to the relatively high binding energy between “Ag–O”; (ii) Chemical replacement is effective to remove these insulating ligands, thus leading to lower contact resistance. Beyond these three strategies, other methods have also been tried, including mechanical rolling, [67, 91] or bending (which is similarly to compressing) [68], silver nanoparticle welding [66], etc. As for the bending treatment, it is usually used to determine the flexibility of TCs or devices, thus usually seen to deteriorate film conductance of electrode like ITO. However, Xia et al. (2015) found that, bending treatment could sharply increase the film conductance of AgNWs TCs [68]. In more, the improvement was found to be sensitive to bending direction. Inner bending (or nanowires are put to the inner side of the bended circle) produced better film conductance. Finally, with the assistance of ultra-long AgNWs,  $R_{sh}$  of 12.5  $\Omega/\square$  was obtained at T% of 90.2% (@550 nm) in 2015. The improvement is also due to the improved contact between nanowires.

### 3.3 Stability and Protection

Due to the high surface energy of both AgNW and CuNW, surface atoms are easily to diffusion, cause breakdown problem [81, 86–90], or Rayleigh like instability problem on one hand [33, 92, 93]; On the other hand, bare nanowire TCs could be easily oxidized or corroded in air or harsh electrochemical environment. As a result, protection should be performed. Usually, this was done by depositing another layer of inert material on the NW surface. Here below three methods are introduced. The first one is electroplating. In 2018, Lee and coworkers electroplated nickel layer on silver microgrid using the equipment shown in Fig. 11a [94]. Nickel electroplating helped to achieve 4.3  $\Omega/\square$  in  $R_{sh}$  and 96% in T%. In addition, Ni coated silver grid showed largely upgraded corrosion resistance. As shown in Fig. 11b, even being put in a quite harsh box filled by sulfur (heated by 150 °C) for 60 min, there was less change in the  $R_{sh}$  of the Ni-coated grid. As such, nickel coating is effective in enhance the anti-corrosion ability of Ag. In fact, similar methods have been applied in AgNWs or CuNWs basing TCs [95–99].

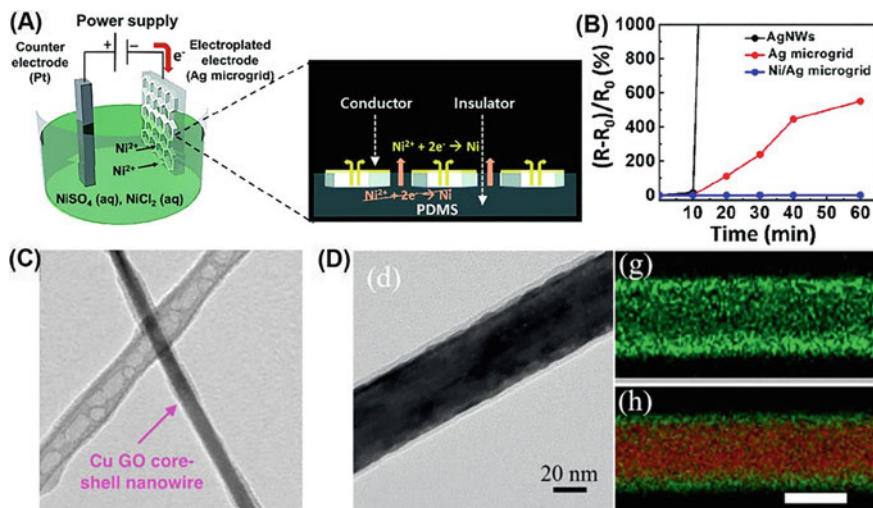


**Fig. 11** **a** Schematic of the electroplating equipment by which silver microgrid electrode embedded in PDMS was coated by thin layer of nickel. **b** Stability test (chemical sulfurization test, 150 °C) on three kinds of electrode basing on AgNWs, Ag microgrid and Ag microgrid coated with nickel layer. Clearly, nickel coated electrode shows the strongest robustness. Reproduced with permission [94]. Copyright © 2013, Royal Society of Chemistry. **c** TEM image of CuNWs wrapped with r-GO layer [100] Reproduced with permission. Copyright 2016, American Chemical Society. **d** TEM image of a typical Ag-Au core—shell nanowire and corresponding EDX mapping (green-Au, red-Ag) [74]

In 2016, Dou et al. wrapped CuNWs by r-GO, which helped to increase both optoelectronic performance and stability of the TCs [100]. The wrapping process could be briefly described. At first, the CuNWs were immersed in graphene oxides (GO) suspension to get core-shell like NWs. Then the GO-wrapped CuNWs were filtrated and transferred to substrate. After that, the sample was annealed in “forming gas” (containing 10%  $\text{H}_2$  in Ar) to reduce GO, which led to r-GO wrapped core-shell CuNWs, as shown in Fig. 11c. Such treatment could improve the optoelectronic performance to 89.3% (T%) and 28.2  $\Omega/\square$  ( $R_{sh}$ ), along with low haze of ~2%. Moreover, storage-stability of 200 days was achieved.

In 2021, Huang et al. reported a kind of Ag-Au core-shell nanowire [74]. During experiments, AgNWs were added to Au precursor where  $\text{HAuCl}_4$  was used as the Au source, and kept in room temperature for about 6 h. The reduced Au atoms were observed to deposit on the surface of AgNWs, with thickness of several nanometers. Typical TEM image of the resultant sample and corresponding EDX maps could clearly be seen in Fig. 11d. Such decoration was found to improve the robustness of the AgNWs against harsh electrochemical environment.

### 3.4 Conducting Mechanism of Networks Made of 1D Conductive Materials

Different from the conventional conductors basing on continuous films or bulks, above discussed TCs are consisting of randomly arranged nanowires. In fact, they are networks, rather than continuous films. From this point of view, distinctive conducting behavior should be anticipated. Indeed, understanding the conducting behavior of such disordered systems is not only a need for the application of TCs basing on nanowires, but also a classical task in statistical physics. For example, experiments showed that network conductance could be affected by aspect ratio (length/width) [33, 65], density [101, 102] and geometrical parameters [103, 104], and also junction resistance in addition [64, 67]. While on the other hand, from the theoretical aspect, the problem could be ascribed to “stick percolation”, which belongs to the classic percolation systems [105–107]. Then two theories were applied to explain the conducting mechanism. Near percolation threshold, the network conductivity could be described by the scaling formula (7):

$$\sigma \sim (p - p_c)^t, \quad (7)$$

whereas  $p$  is the nanowire density, and  $p_c$  the percolation threshold; while  $t$  is dimension-relating parameter, equaling to 1.33 for 2D system [28, 106, 108]. For region away from threshold, or conducting phase has been stably built up, formula (7) is not applicable. Instead, large gap arises, as has been seen in previous report [109]. For this situation, Kirkpatrick’s Effective Medium Theory (EMT, sometimes noted as effective medium approximation, or EMA) proposed in 1970s seems to give reliable description on the conducting behavior, as seen in formula (8) [110]:

$$g_m = 1 - \frac{1 - p}{1 - 2/z} = (2p - 1)|_{z=4}, \quad (8)$$

whereas  $g_m$ ,  $p$ ,  $z$  is normalized conductivity, existence probability of bonds, and maximum coordination number of nodes in 2D lattice. This theory was also used in AgNWs basing networks [111]. However, as being stated above, the nanowire basing TCs are disordered nanowire networks, rather than continuous films. The conductance should be relating closely to the “conducting paths” in the networks. As such, the formation dynamics and hence the effect of such “conducting paths” on the network conductivity should be considered. Honestly, the importance of conducting paths was noticed in literatures [112–115], though the detailed relationship between conducting path and network conductivity was unclear. This problem was then solved by He et al. (2018), with the assistance of simulation and experiment [116]. As shown in Fig. 12, an algorithm was developed to monitor the formation dynamics of conducting paths and network conductance simultaneously. Obviously, more conducting paths could be formed if area fraction of nanowire or nanowire length increases. What is more, two parameters were defined, or the length-ratio

( $\eta_{cp}$ ) of conducting-path to all nanowires, and normalized network conductivity ( $\sigma$ ). According to the numerical simulation, an equation was obtained, as shown in formula (9):

$$\sigma = k(\eta_{cp} - b). \tag{9}$$

When contact resistance is not considered,  $k, b$  equals to 2 and 0.5 respectively, for 2D networks with maximum coordination of 4 for a node. As shown in Fig. 12f, a line could be drawn according to formula (9), which coincides well with the simulated results. When contact resistance is considered, linear behavior could also be seen between network conductivity ( $\sigma$ ) and length ratio ( $\eta_{cp}$ ), though with smaller slope ( $k$ ). Moreover, such linear relationship was verified by experiments basing on AgNWs networks [116]. As a result, parameter of “ $\eta_{cp}$ ” could be used as a basic topological parameter in describing the conducting behavior of disordered systems [117–119]. In fact, this theory could be named as “Effective Path Theory” (EPT) [120]. This theory differs to previous EMT theory in three aspects: (i) EPT only concerns the

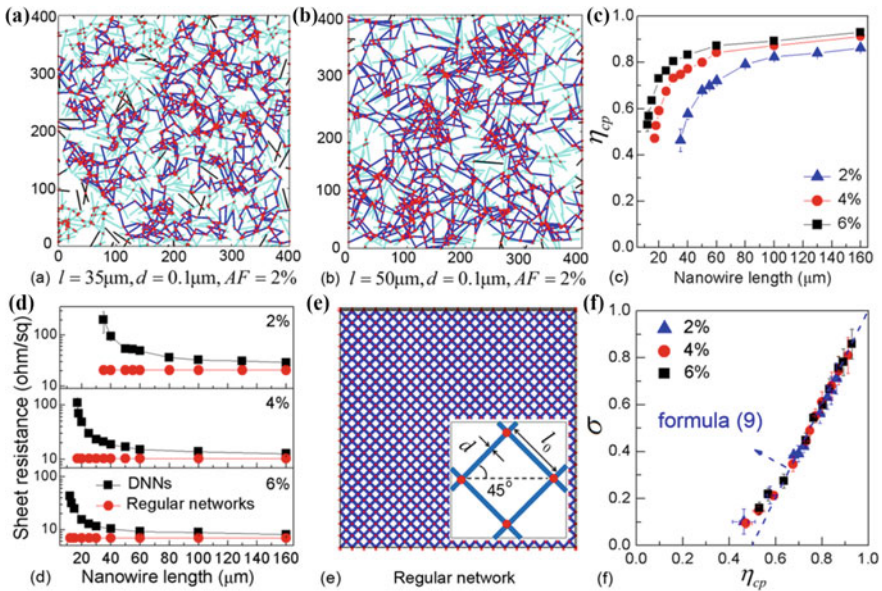


**Fig. 12** Illustration for the suggestion of “Effect-Path Theory” (EPT). Typical 2D disordered nanowire networks (DNNs) simulated from two nanowire lengths: **a** 35  $\mu\text{m}$  and **b** 120  $\mu\text{m}$ . The area fraction (AF) of the nanowires in the network was fixed at 2%. For comparison, the conducting paths are marked by dark blue. Effect of nanowire length on: **c** length-ratio ( $\eta_{cp}$ ) between conducting-path and all nanowires, and **d**  $R_{sh}$  of TC ( $R_{sh}$  of regular networks is plotted for reference). **e** Schematic of regular 2D network. **f** Plotting normalized network conductivity ( $\sigma$ ) against length-ratio ( $\eta_{cp}$ ). Dashed line in (F) shows fitted results according to formula (9) using  $k = 2$  and  $b = 0.5$ . Coincidence could be clearly seen when  $\eta_{cp}$  is larger than 0.6. Reproduced with permission [116]. Copyright 2018, AIP Publishing

formation of conducting paths, which are the collective of the segments in nanowires that really carry current, other than those “dead ends” or branches; while in EMT theory, this could not be distinguished, since the existing probability  $p$  formula (8) contains all of the existing bonds. (ii) The normalization process of EPT is basing on the conductance of a regular network with nanowire width and area fraction equaling to that of disordered nanowire networks; while for EMT, the normalization is basing on regular network with highest area fraction (originally, the normalization is basing on resistor network with existing probability  $p = 1$ . Then if a resistor network is transferred into bond network, “ $p = 1$ ” implies the highest area fraction [110]); (iii) Local conductance or the conductance between neighboring nodes is allowed to vary one by one in EPT, but not so in EMT [110]. However, it is interesting that the two theories share the same mathematic form when comparing the formulas of (8) and (9). Thus further examination is worthy to follow. According to the EPT theory, more attention should be paid to the formation of conducting-paths, in order to obtain higher film conductance.

### 3.5 Applications in Optoelectronic Devices

Immediately after the successful fabrication of TCs, they were introduced to optoelectronic devices, like solar cells, OLED, touch screen, heaters, and so on. Besides, metal nanowires were also used in electromagnetic shielding, sensors, stretchable electronics. Here in this section, the application in optoelectronic devices will be discussed.

#### 3.5.1 Flexible Solar Cells

During the past 10 years, metal nanowires (mainly Ag and Cu) basing TCs have been applied as both top and bottom electrodes in the organic solar cells or perovskite solar cells (typically, OSCs and PSCs). Compared to ITO basing devices, such devices come out with better flexibility, which is appealing for adaptive applications. In addition, when mounted on top, devices could harvest illumination from both top and bottom sides. As such, in the following part, these two kinds of devices are introduced: one is the flexible device, and the other is the semitransparent (Semi-T, for short) device. Typical progresses about the two kinds of solar cells are collected in Tables 3 and 4.

In 2019, a kind of lightweight and flexible PSCs was reported by Kang et al. [125]. As shown in Fig. 13a, they used a very thin (1.3  $\mu\text{m}$  in thickness) and flexible polyethylene naphthalate (PEN) foil as substrate, orthogonally/randomly arranged AgNWs networks were deposited on it, which was used as substrate for PSCs. Power conversion efficiency (PCE) of 15.18% and power-per-weight of 29.4 W/g were achieved for orthogonal network basing TCs. This PCE was close to 16.25% of devices using ITO as TCs, but relative higher than random case (10.3%). The main

**Table 3** Application of metal nanowires basing TCs in flexible solar cells

Nanowire	T <sup>a</sup> (%)	R <sub>sh</sub> ( $\Omega/\square$ )	Subs. <sup>b</sup>	Type of solar cells	Position	PCE (%)	Year
Ag	83	15	–	OSC	Bottom	3.4	2011 [121]
Cu	88	24	Glass	OSC	Bottom	3.1	2014 [122]
Ag	92	7.7	cPI	OSC	Bottom	7.42	2015 [123]
Ag	–	–	PET	PSC	Bottom	13.36	2018 [124]
Ag	92.3	–	PEN	PSC <sup>c</sup>	Bottom	15.18	2019 [125]
Ag	86	11.0	Glass	PSC <sup>d</sup>	Bottom	15.31	2020 [126]
Cu	87.8	34.05	PES	PSC	Bottom	14.18	2020 [127]
Ag	91	22	PET	OSC	Bottom	8.94	2021 [128]
Ag	95 <sup>e</sup>	30 <sup>e</sup>	PEN	PSC module	Bottom & Top	16.78	2020 [129]
Ag	–	–	Ag grid	OSC module	Bottom	16.1 <sup>e</sup>	2021 [130]

<sup>a</sup>Measured at wavelength of 550 nm; <sup>b</sup> substrate when the nanowire network was used as bottom electrode, or bottom electrode when the nanowire network is used as top electrode; <sup>c</sup> lightweight device was prepared; <sup>d</sup> Carbon electrode was adopted as the top electrode; <sup>e</sup>representative data is picked from the literature; <sup>f</sup> OSC module was fabricated basing on a “PET/Ag grid/AgNWs/PEI-Zn” composite electrode; This efficiency was recorded using an aperture with area of 4.095 mm<sup>2</sup>

**Table 1.4** Application of metal nanowires basing TCs in semi-transparency (Semi-T) solar cells

Nanowire	Device	Position	Bottom	T% or AVT	PCE (%)	Test side	Year
Ag	OSC	Top	ITO	66% (T%) <sup>a</sup>	3.82 4.02	Ag ITO	2012[133]
Ag	OSC	Top	ITO	51.8% (T%) <sup>a</sup>	3.15	ITO <sup>b</sup>	2015[134]
Ag	PSC	Top	ITO	23.3% (AVT)	10.45 11.31	Ag ITO	2018[135]

<sup>a</sup>Measured at wavelength of 550 nm; <sup>b</sup>deduced from the literature, or “the top AgNWs TC was sealed before the efficiency test”

difference comes from the short circuit current density ( $J_{SC}$ ). It is 20.09 mA/cm<sup>2</sup> (ITO), 18.63 mA/cm<sup>2</sup> (orthogonal) and 14.88 mA/cm<sup>2</sup> (random) for the three cases as shown in Fig. 13b. The authors ascribed the improved charge collection to the uniform surface of orthogonal AgNWs network. Since this could help to grow uniform perovskite (the photo-active layer, basing on organic lead halide). Also, AgNWs arrangement also affected device stability. For example, after being stored by 500 h, 85% of device efficiency was retained for orthogonal case device, while only 50% was retained for random case. Again, this was also contributed by the improved surface quality of the orthogonal network. In more, after bending at radius of 5 mm for 1000 cycles, about 90% of the start efficiency could be attained. Noting that, conducting polymer of PH1000 was used to modify the AgNW TCs, which makes



the TC more conductive. However, PH1000 was observed to cause degradation on AgNWs, thus protection is needed [131].

CuNW TCs were also used in solar cells. Yang et al. (2020) prepared flexible PSCs on Al-doped ZnO (AZO) protected CuNW TCs [127]. As shown in Fig. 13b, AZO layer was coated on CuNWs by atom layer deposition (ALD) method. By tuning the Al dopant concentration, a composition-gradient AZO (g-AZO) was deposited. Such g-AZO was suggested to be favorable to device performance. It protected nanowire from being corroded by thermal treatment or chemical reactions, thus improve device stability on one hand; and provided gradient energy band alignment, and accelerate charge extraction, reduce recombination on the other hand. Subsequently, g-AZO helped flexible PSCs obtain PCE of 14.18%, close to that of ITO/PEN basing devices (16.33%), while superior to 12.34% of the device assembled from mono-AZO treated CuNWs. Again, excellent robustness was observed. 98% of the start efficiency could be attained after bending at radius of 12.5 mm for 800 cycles, compared to the sharp decrease of ITO basing devices.

More impressively, solar cell modules have also been successfully fabricated using metal nanowire basing electrodes. Gao and Meng (2020) showed that, PSC module could be fully prepared by inkjet printing, including both bottom and top electrodes, light-active layer, electron-transporting layer and hole-transporting layer [129, 132]. As shown in Fig. 14a, modules with size of 120–180 cm<sup>2</sup> were prepared. Such modules showed excellent power conversion efficiencies, or 16.78% for 120

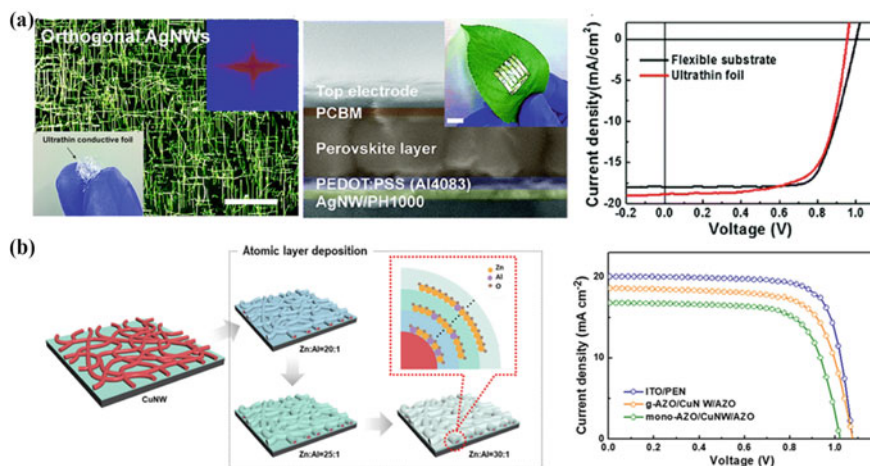


**Fig. 13** Typical applications of metal nanowire basing TCs in flexible solar cells. **a** Flexible organic photovoltaic cell (OSC) assembled from AgNWs TC. The TC was made of cross-linked AgNWs on 1.3  $\mu\text{m}$ -thick PEN foil; typical device structure and current density—voltage (JV) curves are shown on the right side of **a**. Reproduced with permission [125]. Copyright © 2013, Royal Society of Chemistry. **b** Flexible perovskite solar cell (PSC) assembled from CuNWs TC which was coated by gradient-AZO (g-AZO). Typical JV curves are shown on the right side of **b**. Reproduced with permission [127]. Copyright 2020, American Chemical Society

cm<sup>2</sup> module, and 12.56, 10.68% for 150 and 180 cm<sup>2</sup> modules, respectively [129]. Moreover, less hysteresis and prolonged photo-stability were achieved [Fig. 14a]. Modules of organic photovoltaic cells (or organic solar cells, OSCs) have also been prepared using metal nanowire basing TCs. Zhou et al. (2021) fabricated large-area flexible OSC modules with size up to 54 cm<sup>2</sup>, basing on a kind of composite flexible electrode [130]. As shown in Fig. 10b, typically the composite electrode used highly conductive Ag grid/PET as substrate ( $R_{sh} \sim 1.1 \Omega/\square$ ), which had large void space with size up to 100  $\mu\text{m}$ . Then, “AgNWs/ PEI-Zn” (noting PEI-Zn is the short form of “zinc-chelated polyethylenimine”) was used to fill the void and enhance the charge collection of the solar cell. They checked the relation between  $R_{sh}$  of such “AgNWs/PEI-Zn” film (rather than the whole electrode) and the final device performance, and found that, when  $R_{sh}$  was as high as 600  $\Omega/\square$ , PCE of 14.06% was achieved. Decreasing  $R_{sh}$  to 100  $\Omega/\square$  could harvest PCE of 14.74%. Such phenomenon is different to those devices basing on pure AgNWs TCs, though could be ascribed to the usage of highly conductive Ag grid. In more, the “PEI-Zn” itself is conductive. It not only flattens the surface of AgNW TCs, but also improves the thermal stability of the AgNWs basing electrode. Finally, small OSC device with efficiency of 16.1% (active area 4.095 mm<sup>2</sup>), large area single device with efficiency of 13.1% (6 cm<sup>2</sup>), 12.6% (10 cm<sup>2</sup>) and module with efficiency up to 13.2% (54 cm<sup>2</sup>) were achieved, along with excellent flexibility. Besides, flexible quantum-dots light-emitting diodes (QLEDs) with external quantum efficiency up to 13.3% were also successfully fabricated using such composite electrode.

### 3.5.2 Semitransparent Solar Cells

Beside flexible devices, other unique type of solar cells was also proposed. For example in 2012, visibly transparent (or Semi-T) polymer solar cells were reported by Chen et al. (2012), using AgNWs basing TC as top electrode [133]. As shown in Fig. 15a, owing to the excellent transparency of both ITO and AgNWs TC, the device actually open “windows” from both of the two sides. In more, the light-active layer is only sensitive to ultraviolet (UV) and near infrared (NIR) wavelengths. Consequently, the full device is actually “transparent” to our eyes. According to the authors, transparency of the device could reach 66% at 550 nm [middle of Fig. 15a]. However, such transparent device could generate power from irradiations. Even under illumination of AM 1.5G (100 mW/cm<sup>2</sup>, including UV, NIR, and visible wavelengths), it showed power conversion efficiency (PCE) of 4.02, and 3.82%, when it was illuminated from ITO or AgNWs TC sides. Thus, the power conversion property varies little. Following that, several works were performed. Typically, semitransparent OSC modules were reported by Guo et al. (2015), using AgNWs TCs as the top electrode [134]. As shown in Fig. 15b, the photoactive layer derived from the mixture between pDPP5T—2:PC<sub>60</sub>BM enables highly transparency around visible regions in the spectrum.

And series connected modules were prepared using laser pattern technique, using either rigid glass or flexible PET as substrates. Similarly, such modules could generate

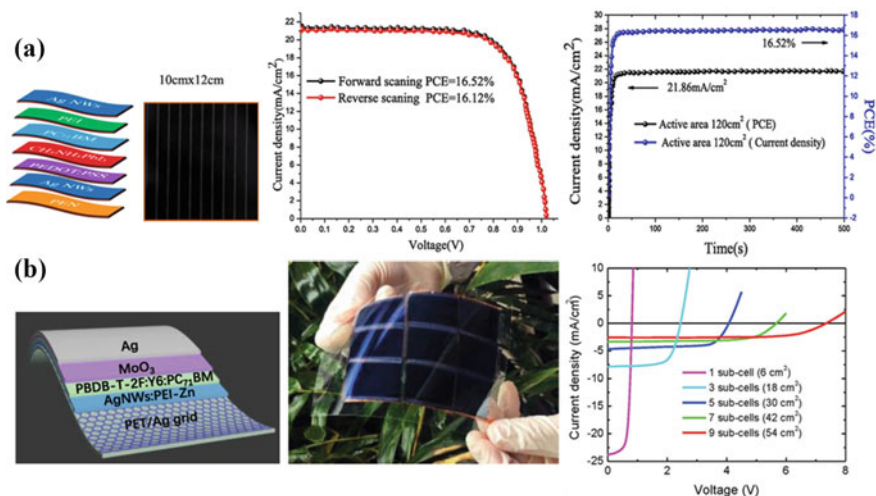


**Fig. 14** Typical applications of metal nanowire based TCs in flexible solar cells modules. **a** Flexible PSC modules assembled with AgNW TCs as both bottom and top electrodes. Typical device structure, module image, JV curves, along with photo-stability test curves is shown on the right side of **a**. Reproduced with permission [129]. Copyright @ 2021, Elsevier. **b** Flexible OSC modules assembled with basing on a “PET/Ag grid/AgNWs/PEI-Zn” composite electrode; Typical device structure, module image, JV curves are shown on the right side of **b**. Reproduced with permission [130]. Copyright @ 2021, John Wiley and Sons

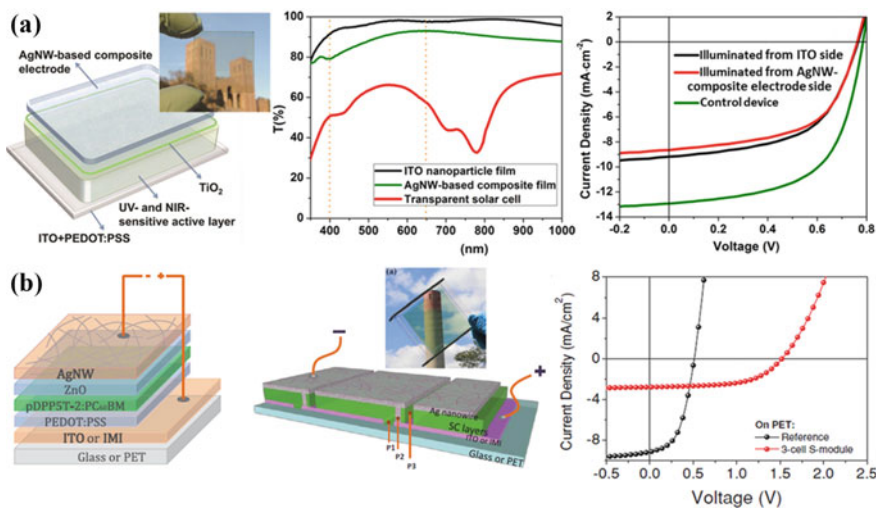


**Fig. 15** Typical applications of metal nanowire based TCs in semitransparent solar cells. **a** Semi-T OSC prepared using AgNWs TC as top electrode. Reproduced with permission [133]. Copyright @ 2012, American Chemical Society. **b** Semi-T OSC module prepared using AgNWs TC as top electrode. Reproduced with permission [134]. Copyright @ 2015, John Wiley and Sons

power from the UV and NIR wavelengths, coming out with PCE of 2.31% for single cell (with active area of  $0.1 \text{ cm}^2$ ), and 2.00% for 10-cell module (with active area of  $1.6 \text{ cm}^2$ ). Noting that T% of the full devices was about 51.8% (@550 nm). In addition, the efficiencies could be upgrade to 3.15 and 2.25% for devices fabricated on glass substrate. Such performance is appealing for daily use. For example, such Semi-T devices could be mounted on windows, as the visible light could pass through, while the other part could generate power. Besides OSCs, such Semi-T perovskite solar cells (PSCs) were also prepared using electrode couple of “ITO/AgNW TC”. For example, Han et al. (2018) prepared Semi-T PSCs by spray-coating AgNW/ZnO nano particles composite electrode on top of devices [135]. The device showed average transmission (AVT) of 23.3% between wavelengths of 400–800 nm, and outcome PCE of 10.45% when illuminated from AgNW side, comparing to 11.31% for the illuminated from ITO side. Anyway, it is worthy to note that, lead halide hybrid perovskite layer (for example,  $\text{MAPbI}_3$ ) usually shows high extinction behavior of the in short wavelengths (<560 nm) [138], thus the semitransparent region is applicable to longer wavelengths, which differs from those Semi-T OSCs.

In fact, using metal nanowire basing TCs becomes a hot topic in recent years. Relate progress could further refer to many publications [3, 5, 8, 136–139]. These works show that, metal nanowires basing TCs could be used as electrodes in thin film photovoltaic techniques.

### 3.5.3 Other Applications

Metal nanowire basing TCs have also been applied in other optoelectronic devices, like OLEDs, touch panels, heater, etc. For example, AgNW TCs were used by Lee et al. (2014) to fabricate flexible OLEDs [140]. Typically, the TCs were prepared by spin-coating AgNWs (with length of 10–20  $\mu\text{m}$  and width of 20–40 nm) on either glass or PEN. Optoelectronic performance of 92.2% (T% @550 nm) and  $10 \Omega/\square$  ( $R_{\text{sh}}$ ) was obtained. Then the hole injection layer, hole transport layer, emission layer, hole blocking layer, electron transport layer, LiF and top Al electrode were mounted in sequence. As shown in Fig. 16a, OLED assembled from AgNW basing TC showed similar electroluminescence spectrum like that basing on ITO electrode. In addition, these devices also produced comparable current efficiencies, and power efficiencies. AgNW TCs were also imported to prepare flexible touch screens. As shown in Fig. 16b, Cho et al. (2017) prepared TCs with cross-aligned AgNWs by large-scale bar-coating method [141]. Noting that this method could help to fabricate large area ( $20 \times 20 \text{ cm}^2$ ) TCs, with optoelectronic performance of 95.0% (T%) and  $21.0 \Omega/\square$  ( $R_{\text{sh}}$ ). And then, force-sensitive touch screens were equipped, and linked to computer system. Similar works were done for application in LED [142, 143], or touch screens [65, 136, 137].

Kim et al. (2013) showed that, metal nanowire TCs could be used as transparent film heaters [144]. As shown in Fig. 17, after coating AgNWs on a large piece of PET, a heater with area of  $250 \times 200 \text{ mm}^2$  was obtained by coating two parallel electrodes on the counter sides. After bias was added between the two electrodes, current

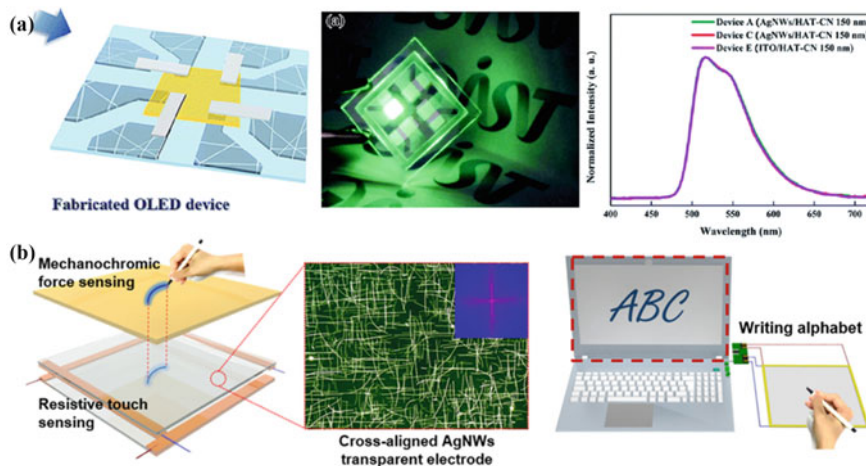


**Fig. 16** **a** Application of AgNW TC in OLEDs. Reproduced with permission [140]. Copyright @ 2009, Royal Society of Chemistry. **b** Application of AgNW TC in touch screens. Reproduced with permission [141]. Copyright @ 2017, American Chemical Society

could be generated, by which joule heat was produced. They tested the temperature on the heater, and found that the temperature distribution was sensitive to nanowire distributions. Hotspots appeared at nanowire aggregations, while uniform distribution was seen at uniformly arranged networks. This heating functionality could be used to defrost. Also shown in Fig. 17b, the frost (formed by keeping film in a refrigerator for 30 min) loaded on surface of AgNW TC could be cleared in just one min, given voltage of 12 V. Moreover, relationship between the temperature, sheet resistance and voltage was studied. As could be anticipated, lower resistance and higher voltage is beneficial for achieving higher temperatures. In fact, the ability of “defrosting” is appealing for daily life, especially for windows, glasses. This has become another important application branch. More works could be found in recently published documents [9, 10, 30].

### 3.6 Summary

In this section, application of metal nanowire in TCs are described, including the method to prepare such TCs, the treatment to improve the optoelectronic properties of the TCs, and also the understanding towards the unique conducting mechanism of such networks. Right now, the main tasks of these TCs are lying on three cases: (i) method to protect nanowires from breakdown caused by surface diffusion, or oxidation and corrosion from outside environment; (ii) method to further decrease contact resistance between nanowires; and (iii) further understanding of the conducting behavior. Silver and copper nanowire TCs have been widely used in



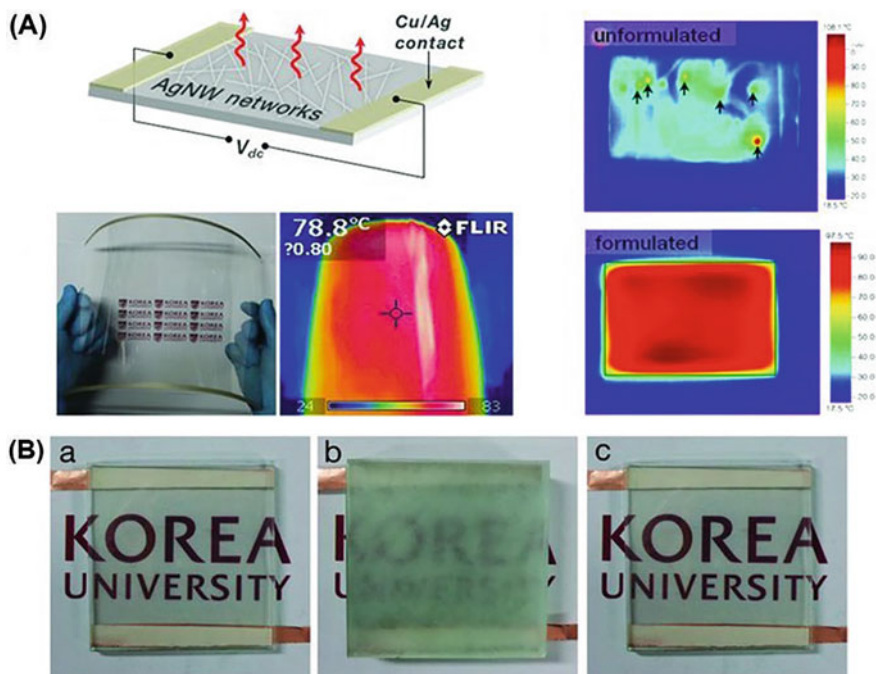


**Fig. 17** Application of AgNW TC in transparent film heaters. **a** Schematic of transparent heater based on AgNW TC; **b** defrosting test of the heater, photo images are shown for: **a** pristine TC, **b** after frost formation, and **c** after heating at 12 V for 60 s. Reproduced with permission [144]. Copyright © 2012, John Wiley and Sons

photoelectronic devices including flexible solar cells, Semi-T solar cells, OLEDs, touch screens and heaters. High transparency, highly conductive and sound flexibility of nanowire basing TCs have opened new windows of these applications. To benefit the applications, right now, the main task might be lying on three cases: (i) In order to favor the charge transport (extraction or injection) process, surface of the nanowire basing TCs should be flattened, while keeping conductive in every position of the surface, including the void space between nanowires; (ii) Due the complex application environment, the nanowires are easily corroded, thus the protection or passivation methods are needed; (iii) Large-area production with incorporation of device modules.

## 4 Perspective

As long as the application in transparent conductor (TC) is considered, AgNWs and CuNWs are the mostly used candidates. These TCs have shown excellent optoelectronic performance, comparable or even superior to commonly used ITO, and better



flexibility, enabling the fabrication of flexible and ultrathin photoelectric devices like solar cells, OLED, touch screens, heaters, and so on. To prompt the application of such nanowire basing TCs, more works are needed, for example, growth method of nanowires and the beneath reaction mechanism, protection towards these thin nanowires, conducting mechanism of random nanowire networks, surface roughness reduction of TC, homogenization on surface conduction, and also the large-area production of device modules. In more, new applications are welcome.

**Acknowledgements** C. Zhou thanks the financial support of National Scientific Foundation of China (NSFC, No. 61774170) and the Natural Science Foundation of Hunan Province (NO. 2020JJ4759). Y. Gao thanks support from National Science Foundation, United States (NSF, DMR-1903962).

## References

1. Zhang R, Engholm M, Hummelgård M, Andersson H, Örtengren J, Olin H, Appl ACS (2018) *Energ Mater* 1:7191
2. Xia YN, Yang PD, Sun YG, Wu YY, Mayers B, Gates B, Yin YD, Kim F, Yan YQ (2003) *Adv Mater* 15:353
3. Scardaci V (2021) *Appl Sci* 11:8035
4. Hu LB, Wu H, Cui Y (2011) *MRS Bull* 36:760
5. Tan DC, Jiang CM, Li QK, Bi S, Song JH (2020) *J Mater Sci Mater Electron* 31:15669
6. Yao S, Zhu Y (2015) *Adv Mater* 27:1480
7. Xu X, Han G, Yu H, Jin X, Yang J, Lin J, Ma C (2019) *J Phys D Appl Phys* 53:05LT02
8. Angmo D, Krebs FC (2013) *J Appl Polym Sci* 129:1
9. Moreira IP, Sanivada UK, Bessa J, Cunha F, Fangueiro R (2021) *Molecules* 26:3685
10. Papanastasiou DT, Schultheiss A, Munoz-Rojas D, Celle C, Carella A, Simonato JP, Bellet D (2020) *Adv Funct Mater* 30:1910225
11. Li Y, Cui F, Ross MB, Kim D, Sun Y, Yang P (2017) *Nano Lett* 17:1312
12. Alia SM, Pivovar BS, Yan Y (2013) *J Am Chem Soc* 135:13473
13. Lyu Z, Xie M, Aldama E, Zhao M, Qiu J, Zhou S, Xia Y, Appl ACS (2019) *Nano Mater* 2:1533
14. Chen ZH, Fang R, Li W, Guan J (2019) *Adv Mater* 31:1900756
15. Feng Y, Zhu J (2019) *Sci China-Mater* 62:1679
16. Gong S, Yap LW, Zhu B, Cheng W (2020) *Adv Mater* 32:1902278
17. Fievet F, Lagier JP, Figlarz M (1989) *MRS Bull* 14:29
18. Silvert PY, Tekaiia-Elhsissen K (1995) *Solid State Ionics* 82:53
19. Silvert P-Y, Herrera-Urbina R, Tekaiia-Elhsissen K (1997) *J Mater Chem* 7:293
20. Fievet F, Lagier JP, Blin B, Beaudoin B, Figlarz M, Ionics SS (1989) 32–33. Part 1:198
21. Zhang QM, Li Y, Xu DS, Gu ZN (2001) *J Mater Sci Lett* 20:925
22. Sloan J, Wright DM, Bailey S, Brown G, York APE, Coleman KS, Green MLH, Hutchison JL, Woo H-G (1999) *Chem Comm* 699
23. Govindaraj A, Satishkumar BC, Nath M, Rao CNR (2000) *Chem Mater* 12:202
24. Braun E, Eichen Y, Sivan U, Ben-Yoseph G (1998) *Nature* 391:775
25. Sun Y, Yin Y, Mayers BT, Herricks T, Xia Y (2002) *Chem Mater* 14:4736
26. Sun Y, Xia Y (2002) *Adv Mater* 14:833
27. Sun Y, Gates B, Mayers B, Xia Y (2002) *Nano Lett* 2:165
28. Xia Y, Xiong Y, Lim B, Skrabalak SE (2009) *Angew Chem Int Edit* 48:60
29. Zheng Y, Zeng J, Ruditskiy A, Liu M, Xia Y (2014) *Chem Mater* 26:22

30. Liu Q, Tian B, Liang J, Wu W (2021) *Mater Horiz* 8:1634
31. Patil JJ, Chae WH, Trebach A, Carter KJ, Lee E, Sannicolò T, Grossman JC (2021) *Adv Mater* 33:2004356
32. Lee E-J, Chang M-H, Kim Y-S, Kim J-Y (2013) *APL Mater* 1:042118
33. Xu X, He S, Zhou C, Xia X, Xu L, Chen H, Yang B, Yang J (2016) *RSC Adv* 6:105895
34. Yang Z, Qian H, Chen H, Anker JN (2010) *J Colloid Interface Sci* 352:285
35. Hong BH, Bae SC, Lee CW, Jeong S, Kim KS (2001) *Science* 294:348
36. Wiley B, Herricks T, Sun YG, Xia YN (2004) *Nano Lett* 4:1733
37. Lee JH, Lee P, Lee D, Lee SS, Ko SH (2012) *Cryst Growth Des* 12:5598
38. Jiu J, Sugahara T, Nogi M, Suganuma K (2013) *J Nanopart Res* 15:1588
39. Gao Y, Jiang P, Liu DF, Yuan HJ, Yan XQ, Zhou ZP, Wang JX, Song L, Liu LF, Zhou WY, Wang G, Wang CY, Xie SS (2003) *Chem Phys Lett* 380:146
40. Gao Y, Song L, Jiang P, Liu LF, Yan XQ, Zhou ZP, Liu DF, Wang JX, Yuan HJ, Zhang ZX, Zhao XW, Dou XY, Zhou WY, Wang G, Xie SS, Chen HY, Li JQ (2005) *J Cryst Growth* 276:606
41. Sun Y, Mayers B, Herricks T, Xia Y (2003) *Nano Lett* 3:955
42. Niu G, Liu F, Yang Y, Fu Y, Wang W (2020) *Colloid Surf A Physicochem Eng Asp* 607:125490
43. Yu Y, Cui F, Sun J, Yang P (2016) *Nano Lett* 16:3078
44. Wiley B, Sun YG, Mayers B, Xia YN (2005) *Chem Eur J* 11:454
45. Caswell KK, Bender CM, Murphy CJ (2003) *Nano Lett* 3:667
46. Gao P-Y, Kunath W, Gleiter H, Weiss K, *Phys Z* (1989) D-Atoms. *Mol Clust* 12:119
47. Hall BD, Flueli M, Monot R, Borel J-P (1991) *Phys Rev B* 43:3906
48. Bovin JO, Alfredsson V, Karlsson G, Carlsson A, Blum Z, Terasaki O (1996) *Ultramicroscopy* 62:277
49. Szpunar B, Erb Palumbo U, Aust KT, Lewis LJ (1996) *Phys Rev B* 53:5547
50. Gryaznov VG, Heydenreich J, Kaprelov AM, Nepijko SA, Romanov AE, Urban J (1999) *Cryst Res Technol* 34:1091
51. Zhang W, Liu Y, Cao R, Li Z, Zhang Y, Tang Y, Fan K (2008) *J Am Chem Soc* 130:15581
52. Im SH, Lee YT, Wiley B, Xia Y (2005) *Angew Chem Int Edit* 44:2154
53. Zhang WJ, Chen P, Gao QS, Zhang YH, Tang Y (2008) *Chem Mater* 20:1699
54. Li B, Ye S, Stewart IE, Alvarez S, Wiley BJ (2015) *Nano Lett* 15:6722
55. Chen DP, Qiao XL, Qiu XL, Chen JG, Jiang RZ (2010) *J Colloid Interface Sci* 344:286
56. Chen D, Zhu G, Zhu X, Qiao X, Chen J (2011) *J Mater Sci Mater Electron* 22:1788
57. Foresti ML, Innocenti M, Kobayashi H, Pezzatini G, Guidelli R (1996) *J Chem Soc Faraday Trans* 92:3747
58. Molares MET, Hühberger EM, Schaefflein C, Blick RH, Neumann R, Trautmann C (2003) *Appl Phys Lett* 82:2139
59. Shi Y, Li H, Chen L, Huang X (2005) *Sci Technol Adv Mater* 6:761
60. Zhang DQ, Wang RR, Wen MC, Weng D, Cui X, Sun J, Li HX, Lu YF (2012) *J Am Chem Soc* 134:14283
61. Cui F, Yu Y, Dou L, Sun J, Yang Q, Schildknecht C, Schierle-Arndt K, Yang P (2015) *Nano Lett* 15:7610
62. Jin M, He G, Zhang H, Zeng J, Xie Z, Xia Y (2011) *Angew Chem Int Edit* 50:10560
63. Lee J-Y, Connor ST, Cui Y, Peumans P (2008) *Nano Lett* 8:689
64. Garnett EC, Cai W, Cha JJ, Mahmood F, Connor ST, Greyson Christoforo M, Cui Y, McGehee MD, Brongersma ML (2012) *Nat Mater* 11:241
65. Lee J, Lee P, Lee H, Lee D, Lee SS, Ko SH (2012) *Nanoscale* 4:6408
66. Lu H, Zhang D, Ren X, Liu J, Choy WCH (2014) *ACS Nano* 8:10980
67. Lee SJ, Kim Y-H, Kim JK, Baik H, Park JH, Lee J, Nam J, Park JH, Lee T-W, Yi G-R, Cho JH (2014) *Nanoscale* 6:11828
68. Xia X, Yang B, Zhang X, Zhou C (2015) *Mater Res Express* 2:075009
69. Ge Y, Duan X, Zhang M, Mei L, Hu J, Hu W, Duan X (2018) *J Am Chem Soc* 140:193
70. Niu Z, Cui F, Kuttner E, Xie C, Chen H, Sun Y, Dehestani A, Schierle-Arndt K, Yang P (2018) *Nano Lett* 18:5329

71. Xu J, Wang K, Li Y, Zhuang T-T, Gao H-L, Liu Y-Y, He C-X, Yu S-H (2020) *Sci China-Chem* 63:1046
72. Hwang H, Kim A, Zhong Z, Kwon H-C, Jeong S, Moon J (2016) *Adv Funct Mater* 26:6545
73. Zhong Z, Woo K, Kim I, Hwang H, Kwon S, Choi Y-M, Lee Y, Lee T-M, Kim K, Moon J (2016) *Nanoscale* 8:8995
74. Huang S, Liu Y, Jafari M, Siaj M, Wang H, Xiao S, Ma D (2021) *Adv Funct Mater* 31:2010022
75. Niu Z, Cui F, Yu Y, Becknell N, Sun Y, Khanarian G, Kim D, Dou L, Dehestani A, Schierle-Arndt K, Yang P (2017) *J Am Chem Soc* 139:7348
76. Deshmukh R, Calvo M, Schreck M, Tervoort E, Sologubenko AS, Niederberger M (2018) *Acs Appl Mater Interfaces* 10:20748
77. Wang J, Chen H, Zhao Y, Zhong Z, Tang Y, Liu G, Feng X, Xu F, Chen X, Cai D, Kang J (2020) *Acs Appl Mater Interfaces* 12:35211
78. Zhang Y, Guo J, Xu D, Sun Y, Yan F (2018) *Nano Res* 11:3899
79. Zhang Y, Guo J, Xu D, Sun Y, Yan F (2018) *Langmuir* 34:3884
80. Xiang H, Guo T, Xu M, Lu H, Liu S, Yu G, Appl ACS (2018) *Nano Mater* 1:3754
81. Song T-B, Chen Y, Chung C-H, Yang Y, Bob B, Duan H-S, Li G, Tu K-N, Huang Y (2014) *ACS Nano* 8:2804
82. Selzer F, Floresca C, Knepe D, Bormann L, Sachse C, Weiß N, Eychmüller A, Amassian A, Müller-L, Leo K (2016) *Appl Phys Lett* 108:163302
83. Dai S, Li Q, Liu G, Yang H, Yang Y, Zhao D, Wang W, Qiu M (2016) *Appl Phys Lett* 108
84. Song C-H, Ok K-H, Lee C-J, Kim Y, Kwak M-G, Han C-J, Kim N, Ju B-K, Kim J-W (2015) *Org Electron* 17:208
85. Jiu J, Sugahara T, Nogi M, Araki T, Suganuma K, Uchida H, Shinozaki K (2013) *Nanoscale* 5:11820
86. Sanders DE, DePristo AE (1992) *Surf Sci* 260:116
87. Khaligh HH, Goldthorpe IA (2013) *Nanoscale Res Lett* 8:235
88. Li Y, Tsuchiya K, Tohyoh H, Saka M (2013) *Nanoscale Res Lett* 8:370
89. Khaligh HH, Xu L, Khosropour A, Madeira A, Romano M, Pradere C, Treguer M, Servant L, Pope MA, Goldthorpe IA (2017) *Nanotechnology* 28:425703
90. Yu H, Jin N, Wang Z, Lin J, Wei J, Luo Q, Ma CQ (2020) *Nanotechnology* 31:18LT01
91. Hauger TC, Al SMI, Buriak JM (2013) *Acs Appl Mater Interfaces* 5:12663
92. Rizza G, Attouchi F, Coulon P-E, Perruchas S, Gacoin T, Monnet I, Largeau L (2011) *Nanotechnology* 22:175305
93. Naik JP, Das K, Prewett PD, Raychaudhuri AK, Chen Y (2012) *Appl Phys Lett* 101:163108
94. Lee K, Park J, Kim H, Park HS, Song HK, Kim KH, Seo K (2018) *J Mater Chem A* 6:11790
95. An S, Jo HS, Kim D-Y, Lee HJ, Ju B-K, Al-Deyab SS, Ahn J-H, Qin Y, Swihart MT, Yarin AL, Yoon SS (2016) *Adv Mater* 28:7149
96. Kang H, Choi S-R, Kim Y-H, Kim JS, Kim S, An B-S, Yang C-W, Myoung J-M, Lee T-W, Kim J-G, Cho JH (2020) *Acs Appl Mater Interfaces* 12:39479
97. Wang S, Tian Y, Hang C, Wang C (2018) *Sci Rep* 8:5260
98. Wang S, Tian Y, Wang C, Hang C (2018) *J Electrochem Soc* 165:D328
99. Zhang L, Chen Y, Xu C, Liu Z, Qiu Y (2018) *RSC Adv* 8:14532
100. Dou L, Cui F, Yu Y, Khanarian G, Eaton SW, Yang Q, Resasco J, Schildknecht C, Schierle-Arndt K, Yang P (2016) *ACS Nano* 10:2600
101. Hu L, Kim HS, Lee J-Y, Peumans P, Cui Y (2010) *ACS Nano* 4:2955
102. De S, Higgins TM, Lyons PE, Doherty EM, Nirmalraj PN, Blau WJ, Boland JJ, Coleman JN (2009) *ACS Nano* 3:1767
103. Zeng Z, Wang C, Gao J (2020) *J Appl Phys* 127:065104
104. Behnam A, Guo J, Ural A (2007) *J Appl Phys* 102:044313
105. Balberg I, Binenbaum N, Anderson CH (1983) *Phys Rev Lett* 51:1605
106. Li J, Zhang S-L (2010) *Phys Rev E* 81:021120
107. Zvezelj M, Stankovic I (2012) *Phys Rev B* 86:134202
108. Pike GE, Seager CH (1974) *Phys Rev B* 10:1421
109. Bauhofer W, Kovacs JZ (2009) *Compos Sci Technol* 69:1486

110. Kirkpatrick S (1973) *Rev Mod Phys* 45:574
111. O'Callaghan C, da Rocha CG, Manning HG, Boland JJ, Ferreira MS (2016) *Phys Chem Chem Phys* 18:27564
112. Kumar A, Vidhyadhiraja NS, Kulkarni GU (2017) *J Appl Phys* 122:045101
113. Li L, Holland S (2014) *Nanomater Energy* 3:139
114. Wu Z, López E, Buldyrev SV, Braunstein LA, Havlin S, Stanley HE (2005) *Phys Rev E* 71:045101
115. Rossen WR, Mamun CK (1993) *Phys Rev B* 47:11815
116. He S, Xu X, Qiu X, He Y, Zhou C (2018) *J Appl Phys* 124:054302
117. Ponzoni A (2019) *Appl Phys Lett* 114:153105
118. Tarasevich YY, Vodolazskaya IV, Eserkepov AV, Akhunzhanov RK (2019) *J Appl Phys* 125:134902
119. Balberg I (2020) *J Appl Phys* 128:204304
120. Zeng J, Wang Y, Zheng X, Zhou C (2022) *J Phys D Appl Phys* 55:414004
121. Zhu R, Chung C-H, Cha KC, Yang W, Zheng YB, Zhou H, Song T-B, Chen C-C, Weiss PS, Li G, Yang Y (2011) *ACS Nano* 5:9877
122. Sachse C, Weiß N, Gaponik N, Müller L, Eychmüller A, Leo K (2014) *Adv Energy Mater* 4:1300737
123. Kim Y, Ryu TI, Ok K-H, Kwak M-G, Park S, Park N-G, Han CJ, Kim BS, Ko MJ, Son HJ, Kim J-W (2015) *Adv Funct Mater* 25:4580
124. Liu X, Yang X, Liu X, Zhao Y, Chen J, Gu Y (2018) *Appl Phys Lett* 113:203903
125. Kang S, Jeong J, Cho S, Yoon YJ, Park S, Lim S, Kim JY, Ko H (2019) *J Mater Chem A* 7:1107
126. Zhou J, Li S, Lv X, Li X, Li Y, Zheng Y-Z, Tao X (2020) *J Power Source* 478:228764
127. Yang H, Kwon H-C, Ma S, Kim K, Yun S-C, Jang G, Park J, Lee H, Goh S, Moon J (2020) *Acs Appl Mater Interfaces* 12:13824
128. Liu H, Wu J, Fu Y, Wang B, Yang Q, Sharma GD, Keshtov ML, Xie Z (2021) *Thin Solid Films* 718:138486
129. Gao B, Meng J (2021) *Sol Energy* 230:598
130. Qin F, Sun LL, Chen HT, Liu Y, Lu X, Wang W, Liu TF, Dong XY, Jiang P, Jiang YY, Wang L, Zhou YH (2021) *Adv Mater* 33:2103017
131. Wang J, Chen X, Jiang F, Luo Q, Zhang L, Tan M, Xie M, Li Y-Q, Zhou Y, Su W, Li Y, Ma C-Q (2018) *Solar RRL* 2:1800118
132. Gao B, Meng J (2021) *Acta Phys Sin* 70:208801
133. Chen C-C, Dou L, Zhu R, Chung C-H, Song T-B, Zheng YB, Hawks S, Li G, Weiss PS, Yang Y (2012) *ACS Nano* 6:7185
134. Guo F, Kubis P, Przybilla T, Spiecker E, Hollmann A, Langner S, Forberich K, Brabec CJ (2015) *Adv Energy Mater* 5:1401779
135. Han K, Xie M, Zhang L, Yan L, Wei J, Ji G, Luo Q, Lin J, Hao Y, Ma C-Q (2018) *Sol Energ Mat Sol C* 185:399
136. Sun YN, Chang MJ, Meng LX, Wan XJ, Gao HH, Zhang YM, Zhao K, Sun ZH, Li CX, Liu SR, Wang HK, Liang JJ, Chen YS (2019) *Nat Electron* 2:513
137. Li WT, Zhang H, Shi SW, Xu JX, Qin X, He QQ, Yang KC, Dai WB, Liu G, Zhou QG, Yu HZ, Silva SRP, Fahlman M (2020) *J Mater Chem C* 8:4636
138. Ma C, Liu YF, Bi YG, Zhang XL, Yin D, Feng J, Sun HB (2021) *Nanoscale* 13:12423
139. Li D, Lai W-Y, Zhang Y-Z, Huang W (2018) *Adv Mater* 30:1704738
140. Lee H, Lee D, Ahn Y, Lee E-W, Park LS, Lee Y (2014) *Nanoscale* 6:8565
141. Cho S, Kang S, Pandya A, Shanker R, Khan Z, Lee Y, Park J, Craig SL, Ko H (2017) *ACS Nano* 11:4346
142. Kim BS, Won S, Seo J, Jeong SK, Kim C, Kim K-S, Kim SH, Cho SM, Kim J-H (2021) *ACS Appl Mater Inter* 13:26601
143. Kim T, Kang S, Heo J, Cho S, Kim JW, Choe A, Walker B, Shanker R, Ko H, Kim JY (2018) *Adv Mater* 30:1800659
144. Kim T, Kim YW, Lee HS, Kim H, Yang WS, Suh KS (2013) *Adv Funct Mater* 23:1250